

Analytical Model of Nonlinear Fiber Propagation for General Dual-Polarization Four-Dimensional Modulation Formats

Zhiwei Liang, Bin Chen, *Senior Member, IEEE*, Yi Lei, *Member, IEEE*, Gabriele Liga, *Member, IEEE* and Alex Alvarado, *Senior Member, IEEE*

Abstract—Coherent dual-polarization (DP) optical transmission systems encode information on the four available degrees of freedom of an optical field: the two polarization states, each with two quadrature components. Such systems naturally operate based on a four-dimensional (4D) signal space. Having a general analytical model to accurately estimate nonlinear interference (NLI) is key to analyze such transmission systems as well as to study how different DP-4D formats are affected by NLI. However, the available models in the literature are not completely general. They either do not apply to the entire DP-4D formats or do not consider all the NLI contributions. In this paper we develop a model that applies to the entire class of DP-4D modulation formats. Our model takes self-channel interference, cross-channel interference and multiple-channel interference effects into account. As an application of our model, we further study the effects of signal-noise interactions in long-haul transmission via the proposed model. When compared to previous results in the literature, our model is more accurate at predicting the contribution of NLI for both low and high dispersion fibers in single- and multi-channel transmission systems. For the NLI, we report an average gap from split step Fourier simulation results below 0.15 dB. The simulation results further show that by considering signal-noise interactions, the proposed model in long-haul transmission improves the NLI power accuracy prediction by up to 8.5%.

Index Terms—Nonlinear interference model, Four-dimensional modulation formats, Signal-noise interaction, Optical fiber communications

I. INTRODUCTION

In optical communication systems, one of the main challenges is to make efficient use of existing network resources. To achieve this, signal shaping has been investigated in optical fiber communications as an effective approach to achieve high spectral efficiencies (SEs). Shaping can be performed

by changing the probability or position of the constellation points, which is known as probabilistic shaping (PS) [2] and geometrical shaping (GS) [3], resp.

Performing joint shaping over multiple dimensions (e.g., time slots, wavelengths, and spatial dimensions) to achieve large performance gains has received interest in the literature for both the additive white Gaussian noise (AWGN) [4]–[7] and the optical fiber channel [7]–[11]. When constellation shaping tailored to the AWGN channel is used in the nonlinear optical channel, however, a performance penalty is introduced. This penalty is caused by the modulation-dependent nonlinear interference (NLI). This effect was studied for example in [12], [13].

In order to harvest most of the gains in the nonlinear fiber channel, heuristic ideas have been used in the literature. These include for example adding constant-modulus constraints [8], [14] or using shell shaping [10] in the optimization. Albeit such heuristics have the potential to significantly reduce the NLI, to fully maximize the performance in the nonlinear channel, an accurate analytical expression that links the modulation geometry and statistics to the induced NLI power is needed. As shown, e.g., in [15], [16], using the split-step Fourier method (SSFM) for constellation optimization becomes computationally demanding dimensions and moderate modulation cardinalities. Therefore, a general NLI model that allows fast and accurate estimation to capture the effect of NLI is essential for optimizing and analyzing the performance of modulation formats in optical communication systems.

In the last two decades, many analytical nonlinear models have been presented in the literature. The models can be broadly grouped into time-domain and frequency-domain models. Some of the most prominent ones are [17]–[25]. The most popular model is the Gaussian noise (GN) model, which was derived based on the assumption that the signal statistically behaves as Gaussian noise over uncompensated links. Soon after the introduction of the GN model, it was pointed out in [24], [25] that ignoring all modulation-format-dependent terms leads to a substantial NLI overestimation.

To analyze and reduce the limitations of the GN model, a number of modulation format-dependent correction formulas have been proposed, effectively lifting the Gaussianity assumption of the transmitted signal. The first part of Table I shows the details of *traditional* models for 2D modulation formats. As shown in Table I, the models in [24], [26] derived the correction terms including self-channel interference (SCI) and

The work of B. Chen, Y. Lei and Z. Liang are supported by the National Natural Science Foundation of China (No. 62171175 and 62001151), by the Fundamental Research Funds for the Central Universities (No. JZ2022HGTB0262). The work of G. Liga is funded by the EuroTechPostdoc programme and the European Research Council under the European Union's Horizon 2020 research and innovation programme (No. 754462). The work of A. Alvarado is supported by the Netherlands Organisation for Scientific Research (NWO) via the VIDI Grant ICONIC (project number 15685). Parts of this paper have been presented at the *European Conference Optical Communication (ECOC)*, Basel, Switzerland, 2022 [1].

Z. Liang, B. Chen, and Y. Lei are with School of Computer Science and Information Engineering, Hefei University of Technology, Hefei, China (e-mails: {bin.chen,leiyi}@hfut.edu.cn).

G. Liga and A. Alvarado are with Department of Electrical Engineering, Eindhoven University of Technology, Eindhoven, The Netherlands (e-mails: {g.liga,a.alvarado}@tue.nl).

cross-phase modulation (XPM) in time domain. The model in [25] derived all the main NLI effects including SCI, cross-channel interference (XCI)¹ and multiple-channel interference (MCI) were derived in frequency domain. A major drawback of all these traditional models is that they can only be applied to polarization-multiplexed 2D (PM-2D) modulation formats, where two identical 2D formats are used to transmit information independently over the two orthogonal polarizations. PM-2D formats are only a subset of all possible dual-polarization four-dimensional (DP-4D) modulation formats.

In order to fully explore the potential of DP-4D modulation formats in the nonlinear fiber channel, [27] introduced the first 4D NLI model as a tool to efficiently trade-off linear and nonlinear shaping gains. The frequency-domain model in [27] applies only to single-channel scenarios since it only considered SCI. Later in [28], a time-domain model was introduced that considers both SCI and cross-phase modulation (XPM). The model in [28] is only valid for 4D symmetric constellations² and high-dispersion fiber systems (e.g., standard single mode fiber (SMF) in dispersion-uncompensated system). The model in [28] was then extended to take SCI, XCI and MCI into account in [29]. The model in [29] can be used for low dispersion fiber but still makes the assumption of 4D symmetric constellations. Recently, based on [28], a model for arbitrary 4D modulation formats was introduced in [30]. The model in [30] was derived in the time domain but only accounts partially for NLI effects (SCI and XPM terms only). The state-of-the-art NLI models for 4D modulation formats are summarized in the second part of Table I.

The contribution of this paper is twofold. First, we derive an “ultimate” 4D NLI model that covers the entire DP-4D class of modulation formats. We achieve this by extending the 4D NLI model (SCI-only) in [27] to consider all the main NLI contributions, including SCI, XCI and MCI. Secondly, we extend our preliminary results in [1] on signal-noise interactions for single-channel DP-4D systems to wavelength division multiplexed (WDM) systems. We perform a comprehensive numerical analysis in multi-channel WDM systems with three different fibers with different dispersion parameters. Our study is validated by analytically studying the effective signal-to-noise ratio (SNR) using general DP-4D formats. Our results show that the proposed 4D nonlinear model has a superior accuracy with a maximum deviation of 0.15 dB in terms of NLI power for all 4D modulation formats studied in this work. Moreover, by considering the signal-noise interactions in a multi-channel long-haul transmission system, the SNR estimation error can be reduced to 0.1 dB with respect to SSFM results, which can be translated into a 4% prediction accuracy improvement in terms of transmission reach compared with only considering signal-signal interactions.

This paper is structured as follows. In Sec. II, we present the system model and review the effective SNR considering the signal-signal and signal-noise interactions. Sec. III presents the expression of the proposed NLI model and the key steps

¹Recall that there are 4 XCI terms, often called X1, X2, X3, and X4 (see Fig. 2 ahead, where X1 corresponds to XPM).

²Constellations which are symmetric with respect to the origin, and have the same power in both polarizations [28, Sec. I].

TABLE I
NLI MODELS FOR OPTICAL FIBER COMMUNICATION SYSTEMS RELEVANT FOR THIS WORK.

Ref.	SCI	XCI Terms	MCI	Mod. Format	Dispersion	Dom.
2D NLI Model						
[24], [26]	✓	XPM only	✗	PM-2D	High	<i>t</i>
[25]	✓	✓(X1-X4)	✓	PM-2D	Any	<i>f</i>
4D NLI Model						
[27]	✓	✗	✗	DP-4D	Any	<i>f</i>
[28]	✓	✓(XPM only)	✗	Symmetric	High	<i>t</i>
[29]	✓	✓(X1-X4)	✓	Symmetric	Any	<i>t</i>
[30]	✓	✓(XPM only)	✗	DP-4D	High	<i>t</i>
This work	✓	✓(X1-X4)	✓	DP-4D	Any	<i>f</i>

t: time domain; *f*: frequency domain; XPM same as X1 (see Fig. 2)

of its derivation. Sec. IV is devoted to validate this model and assess the contribution of signal-noise interaction via a wide range of 4D modulation formats. Sec. V concludes this paper and outlines the potential direction for future research. Finally, the appendix provides a detailed derivation of the NLI model.

II. SYSTEM MODEL AND PERFORMANCE METRICS

A. System Model

In this work, we consider the equivalent model of an optical fiber system shown in Fig. 1 (a). The physical channel is a multi-span, h -channel WDM fiber system using one Erbium-doped fiber amplifier (EDFA) per span to ideally compensate the span losses. At the transmitter, the input bits are mapped into 4D symbols using a predefined DP-4D modulation format and its corresponding binary labeling. The 4D symbols are pulse-shaped by a real pulse $p(t)$ on x and y polarisation. The 4D transmitted WDM signal under a periodic assumption with period T can be expressed in time domain as

$$E(t, 0) = \sum_{h=1}^{N_{ch}} \tilde{E}(t, 0) e^{j f_c t}, \quad (1)$$

where N_{ch} is the total number of channels and h is the WDM channel-index, f_c is the center frequency of channel. According to the channel of interest (COI) or interference (INT) channel, the 4D transmitted signal over single channel $\tilde{E}(t, 0)$ can be represented as

$$\tilde{E}(t, 0) = \begin{cases} \sum_{n=-(W-1)/2}^{(W-1)/2} \mathbf{a}_n p(t - nT_s), & f_c \text{ is COI} \\ \sum_{n=-(W-1)/2}^{(W-1)/2} \mathbf{b}_n p(t - nT_s), & f_c \text{ is INT} \end{cases}, \quad (2)$$

where $T_s = 1/R_s = T/W$ represents the symbol period. R_s is the symbol rate and W is the number of symbols transmitted every period T . The variable \mathbf{a}_n or \mathbf{b}_n denote that the sequence of symbols are from the COI or INT channel, respectively.

After transmitting the symbols over the physical channel, the received symbols are processed by a receiver DSP block, including chromatic dispersion compensation, matched filtering, sampling and ideal phase compensation for potential constant phase rotation. The symbols are then demapped by a 4D demapper to generate soft information (i.e., log-likelihood ratios), which is then used to estimate the transmitted bits and to get the system performance metrics.

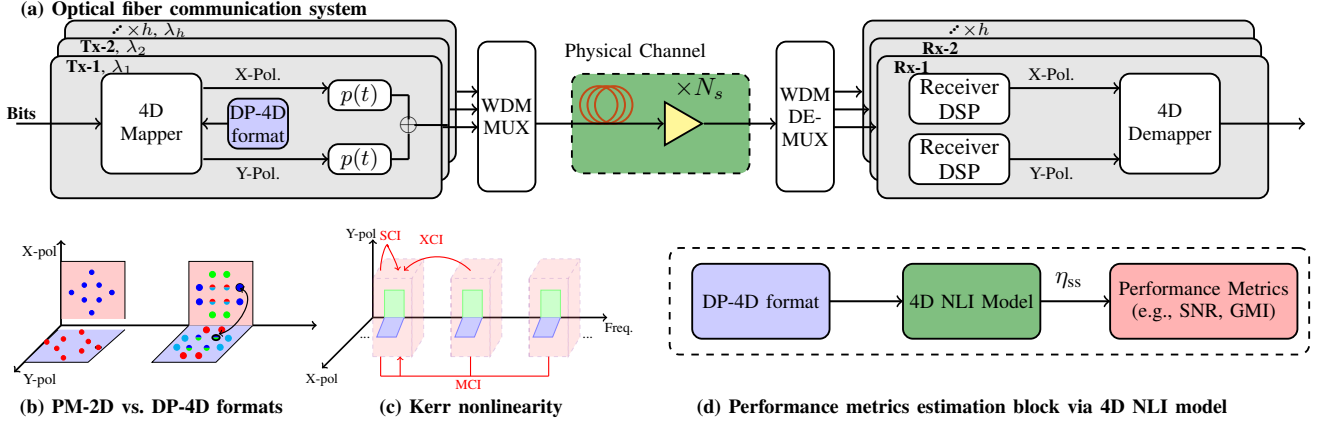


Fig. 1. (a) System model under investigation in this work which consists of a general WDM optical fiber system. (b) PM-2D vs. DP-4D formats. (c) An example of effects experienced by three frequency channels along the modulated dimensions. (d) A general block diagram using NLI model to estimate the modulation-dependent performance metrics.

There are mainly two ways of generating a sequence of 4D symbols. These are schematically shown in the Fig. 1 (b). The left hand side of Fig. 1 (b) shows the case of PM-2D formats, where the 4D points can be described using independent and identically distributed 2D points on each polarization. The right hand side of Fig. 1 (b) show the more general case called DP-4D, where the 2D constellations are jointly modulated on two orthogonal polarization state. In this case, the 2D projections in each polarization are not independent.

B. Performance Metrics

It is known that calculating performance metrics of optical transmission system using SSFM simulations is a time-consuming task. An NLI model can be an efficient way to solve this problem. The general idea is shown in Fig. 1 (d), where the NLI model is used to replace the time-consuming SSFM simulations in order to predict certain performance metrics. To explore the role of signal-noise interactions, in this paper we focus on predicting the effective SNR as well as the generalized mutual information (GMI) [31], [32]. To estimate effective SNR, we will use our proposed model to estimate NLI power coefficients η_{ss} and η_{sn} , which are associated to signal-signal (ss) and signal-noise (sn) components, respectively. As we will show later, these two coefficients are sufficient to estimate the effective SNR in a multi-channel multi-span scenario for arbitrary DP-4D modulation formats. To estimate the GMI, we will use our proposed model to predict the SNR for a given transmission scenario, and then use the Gauss-Hermite approximation to calculate the GMI.

Under an additive NLI noise assumption, the effective SNR over the two polarizations is defined as:

$$\text{SNR}_{\text{eff}}^{\text{model}} \triangleq \frac{P}{N_s \sigma_{\text{ASE}}^2 + \sigma_{ss}^2 + \sigma_{sn}^2}, \quad (3)$$

where P denotes the transmitted signal power per channel, N_s is the number of spans. Assuming ideal transceivers, the main contributions to the total noise power are consisting of three parts: i) amplified spontaneous emission (ASE) noise over one span denoted as σ_{ASE}^2 , ii) signal-signal NLI power denoted as σ_{ss}^2 and iii) signal-ASE noise NLI power denoted as σ_{sn}^2 . The effective SNR in (3) corresponds to the SNR after fiber propagation and the receiver DSP including chromatic dispersion compensation and phase compensation.

For dual-polarized signals over multi-span transmission, the signal-signal NLI power σ_{ss}^2 in (3) can be approximated as [33]

$$\sigma_{ss}^2 \triangleq \sigma_{ss,x}^2 + \sigma_{ss,y}^2 \approx \tilde{\eta}_{ss} N_s^{1+\varepsilon} P^3 = \eta_{ss} P^3, \quad (4)$$

where ε is the so-called NLI coherence factor, which is a function of fiber link parameters (attenuation, dispersion, span length, etc) [34, eq. (40)] and

$$\tilde{\eta}_{ss} \triangleq \tilde{\eta}_{ss,x} + \tilde{\eta}_{ss,y} \quad (5)$$

$$\eta_{ss} \triangleq \eta_{ss,x} + \eta_{ss,y} = \tilde{\eta}_{ss} N_s^{1+\varepsilon}, \quad (6)$$

in which the $\tilde{\eta}_{ss}$ is the signal-signal NLI power coefficient (over one span). As shown in (4), from now on we will use η_{ss} to denote the accumulated signal-signal NLI power coefficient over two polarizations and N_s spans.

The ASE noise generated by the EDFAs leads not only to an additive white Gaussian noise (AWGN) but also to a nonlinear interference produced by the interaction of ASE noise and the transmitted signal [35]. Under the assumption of a flat transmitted signal spectrum and same propagated signal and ASE noise bandwidth, the signal-ASE noise NLI power coefficient can be estimated as $\tilde{\eta}_{sn} = 3\tilde{\eta}_{ss}$, where the $\tilde{\eta}_{sn}$ is the signal-ASE noise NLI power coefficient over one span [36, Sec. 3] [33, eq. (1)]. Thus, by following [36, eq. (8)], the NLI power of signal-ASE noise interactions can be expressed as

$$\sigma_{sn}^2 \triangleq \sigma_{sn,x}^2 + \sigma_{sn,y}^2 = \xi \tilde{\eta}_{sn} \sigma_{\text{ASE}}^2 P^2 = 3\xi \tilde{\eta}_{ss} \sigma_{\text{ASE}}^2 P^2, \quad (7)$$

where

$$\xi = \sum_{n=1}^{N_s} n^{1+\varepsilon} \approx \frac{N_s^{2+\varepsilon}}{2+\varepsilon} + \frac{N_s^{1+\varepsilon}}{2} \quad (8)$$

is the signal-ASE noise NLI accumulation coefficient [36, Sec. 3], and $\tilde{\eta}_{sn}$ denotes the signal-ASE NLI power coefficient (over one span). Note that here the η_{sn} is approximation, while the η_{ss} do not use the same approximation but is computed exactly (in full integral form).

The total NLI power is estimated using (4) (6) (7) and (8). The effective SNR in (3) can then be expressed as

$$\text{SNR}_{\text{eff}}^{\text{model}} \approx \frac{P}{N_s \sigma_{\text{ASE}}^2 + \eta_{ss} P^3 + 3\eta_{ss} \left(\frac{N_s}{2+\varepsilon} + \frac{1}{2} \right) \sigma_{\text{ASE}}^2 P^2}. \quad (9)$$

Note that η_{ss} is a constant value (for a given system configuration) linked to the contributions of both modulation-independent and modulation-dependent nonlinearities. In next

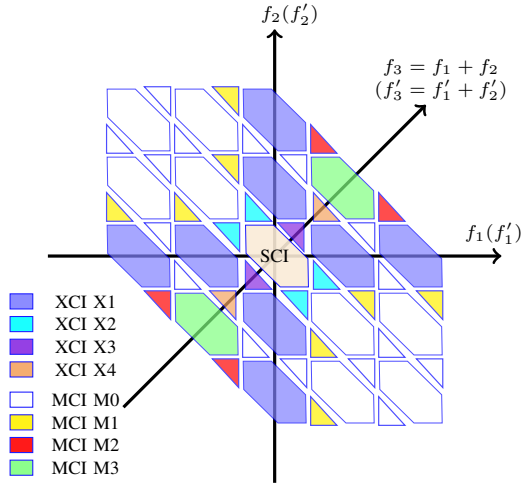


Fig. 2. Example of regions of XCI and MCI for 5 channels at $f = 0$.

section, the NLI power coefficient η_{ss} will be shown including all the main NLI in multi-channel WDM optical systems.

III. THE NONLINEAR MODEL DERIVATION

As shown in Fig. 1 (c), the NLI effects experienced by the transmitted signals in a multi-channel WDM optical system due to the Kerr effect can be categorised using different names depending on the involved channels [37]:

- SCI: NLI caused by the COI on itself.
- XCI: NLI affecting the COI caused by the beating of the COI with any single INT channel. XPM is a subset of the total XCI, namely the XCI contributions in X1.
- MCI: NLI affecting the COI, caused by the beating between frequency components located over two different INT channels or three distinct channels.

The NLI effects can be physically interpreted as the frequency beating of the COI with all other channels through the four-wave mixing (FWM) process. This is reflected in the “link function” which represents the normalized FWM efficiency $\mu(f_1, f_2, f)$ of the three “pump” frequency beatings f_1, f_2 and $f_3 = f_1 + f_2 - f$. In the 4D model formulas, the PSD of the NLI is provided by two triples: (f_1, f_2, f_3) and (f'_1, f'_2, f'_3) . Since for each region in the $[f_1, f_2]$ plane there exist an equivalent region in the $[f'_1, f'_2]$ plane, integrating over regions in the $[f_1, f_2]$ plane is enough [37]. We will now provide a graphical intuitive description assuming $f = 0$ (for simplicity). In Fig. 2, we show the integration regions in the $[f_1, f_2]$ plane needed to obtain the power spectrum of NLI for $f = 0$, for a five-channel WDM system. Here, each island (including lozenge-shaped and triangles) represents a triple of frequencies, namely (f_1, f_2, f_3) . Based on the location of (f_1, f_2, f_3) triples, all different NLI contributions can be fully categorized as XCI: X1, X2, X3 and X4 and MCI: M0, M1, M2 and M3.

In this paper, we follow an approach similar to that of the EGN model [37], i.e., we derive the NLI power coefficient η_{ss} in (6) by first expressing it as

$$\eta_{ss} = \eta_{ss,SCI} + \eta_{ss,XCI} + \eta_{ss,MCI}. \quad (10)$$

The $\eta_{ss,SCI}$ term has been derived in [27]. The other terms will be derived in the following subsections.

A. SCI contribution

In [27], a detailed derivation of the SCI term accounting for DP-4D formats was shown, which has also been validated in [1], [38]. Here, we review the main defining formulas and key conclusions from [27], [38].

For general DP-4D formats, the modulation-dependent coefficient $\eta_{ss,SCI} = \eta_{ss,SCI}^x + \eta_{ss,SCI}^y$ for the x polarization can be calculated using [38, eq. (1)]

$$\begin{aligned} \eta_{ss,SCI}^x = & \left(\frac{8}{9}\right)^2 \frac{\gamma^2}{P^3} \left[R_s^3 (\Phi_1 \chi_1(f) + \Phi_2 \chi_2(f) + \Phi_3 \chi_3(f)) \right. \\ & + R_s^2 (\Psi_1 \chi_4(f) + 2\Re\{\Psi_2 \chi_5(f) + \Psi_3 \chi_5(f)^*\}) \\ & + \Psi_4 \chi_6(f) + 2\Re\{\Lambda_1 \chi_7(f) + \Lambda_2 \chi_7(f)^*\} + \Lambda_3 \chi_8(f) \\ & + 2\Re\{\Lambda_4 \chi_9(f) + \Lambda_5 \chi_9(f)^*\} + \Lambda_6 \chi_{10}(f) \\ & \left. + R_s \Xi_1 \chi_{11}(f) \right], \end{aligned} \quad (11)$$

where γ is the nonlinear coefficient, R_s is the symbol rate, $\Re\{\cdot\}$ denote the real part of a complex number, the coefficients $\Phi_k, k = 1, 2, 3, \Psi_k, k = 1, 2, 3, 4, \Lambda_k, k = 1, 2, \dots, 6$, and Ξ_1 are modulation format-dependent terms as functions of several different intra- and cross-polarization moments, which can be found in Table II. The coefficients $\chi_k, k = 1, 2, \dots, 11$ are given in Table III and are the frequency-dependent integrals over the channel bandwidth. These coefficients are independent with the shape of the modulation format. The expression for $\eta_{ss,SCI}^y$ can be obtained applying the transformation $x \rightarrow y$ and $y \rightarrow x$ to (11).

B. XCI contribution

The XCI contributions of multi-channel WDM systems can be added up independently, and therefore, for simplicity, we only consider a COI whose central frequency is set to zero and an INT channel with central frequency f_c . The total XCI is then the sum of the contributions of each INT channel that exists in the WDM channels. The following Theorem presents the XCI contributions.

Theorem 1: For a generic aperiodic transmitted signal and a WDM fiber transmission system like the one in Fig. 1 (a), the coefficient $\eta_{ss,XCI}^x$ for the x polarization can be written as

$$\begin{aligned} \eta_{ss,XCI}^x = & \left(\frac{8}{9}\right)^2 \frac{\gamma^2}{P^3} \left[R_s^3 [(\Phi_4 + \Psi_5) \chi_{12}(f) + \Phi_5 \chi_{13}(f) \right. \\ & + \Psi_6 \chi_{15}(f) + \Lambda_7 \chi_1(f) + \Lambda_8 \chi_2(f)] \\ & \left. + R_s^2 [(\Phi_6 + \Psi_7) \chi_{14}(f) + \Lambda_9 \chi_{10}(f)] \right] + \bar{\eta}_{ss,SCI}^x, \end{aligned} \quad (12)$$

where the XCI coefficients are given in Table II and Table III, and $\bar{\eta}_{ss,SCI}^x$ is obtained using $\eta_{ss,SCI}^x$ after swapping $a_{x/y} \rightarrow b_{x/y}$ for the coefficients in Table II, and by changing the integration regions $[R_s/2, -R_s/2] \rightarrow [f_c + R_s/2, f_c - R_s/2]$ for the coefficients in Table III.

Proof: See Appendix A. ■

TABLE II
MODULATION FORMAT-DEPENDENT COEFFICIENTS IN (11), (12) AND (13)

Name	Value	SCI	XCI	MCI
Φ_1	$2\mathbb{E}^3\{ a_x ^2\} + 4\mathbb{E}\{ a_x ^2\} \mathbb{E}\{a_x a_y^*}\}^2 + \mathbb{E}\{ a_x ^2\}\mathbb{E}^2\{ a_y ^2\} + \mathbb{E}\{a_x a_y^*}\} ^2 \mathbb{E}\{ a_y ^2\}$	✓		
Φ_2	$4\mathbb{E}\{ a_x ^2\} \mathbb{E}\{a_x^2\} ^2 + \mathbb{E}\{ a_x ^2\} \mathbb{E}\{a_y^2\} ^2 + 4\mathbb{E}\{ a_x ^2\} \mathbb{E}\{a_x a_y}\} ^2 + \mathbb{E}\{a_x a_y}\} ^2 \mathbb{E}\{ a_y ^2\}$ $+ 2\Re\{\mathbb{E}\{a_x a_y}\mathbb{E}\{a_x^* a_y}\mathbb{E}\{a_y^2\} + 2\mathbb{E}^*\{a_x^2\}\mathbb{E}\{a_x a_y}\mathbb{E}\{a_x a_y^*}\}\}$	✓		
Φ_3	$\mathbb{E}\{ a_x ^2\} \mathbb{E}\{a_x^2\} ^2 + \mathbb{E}\{a_x a_y}\} ^2 \mathbb{E}\{ a_y ^2\} + 2\Re\{\mathbb{E}\{a_x^2\}\mathbb{E}^*\{a_x a_y}\mathbb{E}\{a_x^* a_y}\}\}$	✓		
Ψ_1	$4 \mathbb{E}\{a_x a_x ^2\} ^2 + 4 \mathbb{E}\{ a_x ^2 a_y}\} ^2 + \mathbb{E}\{ a_x ^2 a_y\}\mathbb{E}\{a_y^* a_y ^2\} + \mathbb{E}\{ a_x ^2 a_y^*}\mathbb{E}\{a_y a_y ^2\} + \mathbb{E}\{a_x a_y ^2\} ^2$ $+ \mathbb{E}\{a_x^* a_y^2\} ^2 + 2\Re\{\mathbb{E}\{a_x^* a_x ^2\}\mathbb{E}\{a_x a_y ^2\}\}$	✓		
Ψ_2	$2 \mathbb{E}\{a_x a_x ^2\} ^2 + 2 \mathbb{E}\{ a_x ^2 a_y}\} ^2 + \mathbb{E}\{ a_x ^2 a_y^*}\mathbb{E}\{a_y a_y ^2\} + \mathbb{E}\{a_x a_y ^2\} ^2$	✓		
Ψ_3	$\mathbb{E}\{a_x^* a_x ^2\}\mathbb{E}\{a_x a_y ^2\} + \mathbb{E}\{a_x^2 a_y^*}\} ^2$	✓		
Ψ_4	$ \mathbb{E}\{a_x^3\} ^2 + 2 \mathbb{E}\{a_x^2 a_y}\} ^2 + \mathbb{E}\{a_x a_y^2\} ^2$	✓		
Λ_1	$-3\mathbb{E}\{ a_x ^2\} \mathbb{E}\{a_x^2\} ^2 + \mathbb{E}^*\{a_x^2 a_x ^2\}\mathbb{E}\{a_x^2\} - \mathbb{E}\{a_x^2\} ^2 \mathbb{E}\{ a_y ^2\} - 2 \mathbb{E}\{a_x a_y}\} ^2 \mathbb{E}\{ a_y ^2\}$ $+ \mathbb{E}\{a_x^2\}\mathbb{E}^*\{a_x^2 a_y ^2\} - 2\mathbb{E}\{a_x^2\}\mathbb{E}^*\{a_x a_y}\mathbb{E}\{a_x^* a_y}\} + \mathbb{E}\{a_x a_y}\mathbb{E}^*\{a_x a_y a_y ^2\} - \mathbb{E}\{a_x a_y}\mathbb{E}\{a_x^* a_y}\}\mathbb{E}^*\{a_y^2\}$	✓		
Λ_2	$-2\mathbb{E}\{ a_x ^2\} \mathbb{E}\{a_x a_y}\} ^2 + \mathbb{E}\{a_x a_y}\mathbb{E}^*\{a_x a_y a_x ^2\} - \mathbb{E}\{a_x^2\}\mathbb{E}^*\{a_x a_y}\mathbb{E}\{a_x^* a_y}\}$	✓		
Λ_3	$4\mathbb{E}\{ a_x ^4\}\mathbb{E}\{ a_x ^2\} - 4\mathbb{E}\{ a_x ^2\} \mathbb{E}\{a_x^2\} ^2 - 8\mathbb{E}^3\{ a_x ^2\} + 4\mathbb{E}\{ a_x ^2\}\mathbb{E}\{ a_x ^2 a_y ^2\} - 12\mathbb{E}\{ a_x ^2\} \mathbb{E}\{a_x a_y^*}\} ^2$ $- 4\mathbb{E}\{ a_x ^2\} \mathbb{E}\{a_x a_y}\} ^2 - 4\mathbb{E}^2\{ a_x ^2\}\mathbb{E}\{ a_y ^2\} - 3\mathbb{E}\{ a_x ^2\}\mathbb{E}^2\{ a_y ^2\} - \mathbb{E}\{ a_x ^2\} \mathbb{E}\{a_y^2\} ^2 + \mathbb{E}\{ a_x ^2 a_y ^2\}\mathbb{E}\{ a_y ^2\}$ $+ \mathbb{E}\{ a_x ^2\}\mathbb{E}\{ a_y ^4\} - 5 \mathbb{E}\{a_x a_y^*}\} ^2 \mathbb{E}\{ a_y ^2\} - \mathbb{E}\{a_x a_y}\} ^2 \mathbb{E}\{ a_y ^2\} + 2\Re\{2\mathbb{E}\{a_x a_y^*}\mathbb{E}\{a_x^* a_y a_x ^2\}$ $- \mathbb{E}\{a_x a_y}\mathbb{E}\{a_x^* a_y}\}\mathbb{E}^*\{a_y^2\} + \mathbb{E}\{a_x^* a_y}\mathbb{E}\{a_x a_y^* a_y ^2\} - 2\mathbb{E}^*\{a_x^2\}\mathbb{E}\{a_x a_y}\mathbb{E}\{a_x a_y^*}\}\}$	✓		
Λ_4	$-6\mathbb{E}\{ a_x ^2\} \mathbb{E}\{a_x^2\} ^2 + 2\mathbb{E}^*\{a_x^2 a_x ^2\}\mathbb{E}\{a_x^2\} + 4\mathbb{E}\{ a_x ^2\} \mathbb{E}\{a_x a_y}\} ^2 - \mathbb{E}\{ a_x ^2\} \mathbb{E}\{a_y^2\} ^2$ $+ \mathbb{E}^*\{ a_x ^2 a_y^2\}\mathbb{E}\{a_y^2\} + 2\mathbb{E}\{a_x a_y}\mathbb{E}^*\{a_x a_x ^2 a_y\} - 2 \mathbb{E}\{a_x a_y}\} ^2 \mathbb{E}\{ a_y ^2\} - 2\mathbb{E}^*\{a_x^2\}\mathbb{E}\{a_x a_y}\mathbb{E}\{a_x a_y^*}\}$ $+ \mathbb{E}\{a_x a_y}\mathbb{E}^*\{a_x a_y a_y ^2\} - \mathbb{E}^*\{a_x a_y}\mathbb{E}\{a_x a_y^*}\}\mathbb{E}\{a_y^2\} - 2\Re\{\mathbb{E}^*\{a_x a_y}\mathbb{E}\{a_x a_y^*}\}\mathbb{E}\{a_y^2\}\}$	✓		
Λ_5	$-2\mathbb{E}\{ a_x ^2\} \mathbb{E}\{a_x a_y}\} ^2 + \mathbb{E}\{a_x a_y}\mathbb{E}^*\{a_x a_y a_x ^2\} - \mathbb{E}\{a_x^2\} ^2 \mathbb{E}\{ a_y ^2\} - \mathbb{E}^*\{a_x^2\}\mathbb{E}\{a_x a_y}\mathbb{E}\{a_x a_y^*}\}$ $- 2\Re\{\mathbb{E}\{a_x^2\}\mathbb{E}^*\{a_x a_y}\mathbb{E}\{a_x^* a_y}\}\}$	✓		
Λ_6	$-2\mathbb{E}^3\{ a_x ^2\} + \mathbb{E}\{ a_x ^4\}\mathbb{E}\{ a_x ^2\} - \mathbb{E}\{ a_x ^2\} \mathbb{E}\{a_x^2\} ^2 - 4\mathbb{E}\{ a_x ^2\} \mathbb{E}\{a_x a_y^*}\} ^2 - \mathbb{E}\{ a_x ^2\}\mathbb{E}^2\{ a_y ^2\}$ $+ \mathbb{E}\{ a_x ^2 a_y ^2\}\mathbb{E}\{ a_y ^2\} - \mathbb{E}\{a_x a_y^*}\} ^2 \mathbb{E}\{ a_y ^2\} - \mathbb{E}\{a_x a_y}\} ^2 \mathbb{E}\{ a_y ^2\}$ $+ 2\Re\{\mathbb{E}\{a_x a_y^*}\mathbb{E}\{a_x^* a_y a_x ^2\} - \mathbb{E}\{a_x^2\}\mathbb{E}^*\{a_x a_y}\mathbb{E}\{a_x^* a_y}\}\}$	✓		
Ξ_1	$\mathbb{E}\{ a_x ^6\} - 9\mathbb{E}\{ a_x ^4\}\mathbb{E}\{ a_x ^2\} + 12\mathbb{E}^3\{ a_x ^2\} - 2\mathbb{E}\{ a_x ^4\}\mathbb{E}\{ a_y ^2\} + \mathbb{E}\{ a_x ^2 a_y ^4\} - 8\mathbb{E}\{ a_x ^2\}\mathbb{E}\{ a_x ^2 a_y ^2\}$ $- 4\mathbb{E}\{ a_x ^2 a_y ^2\}\mathbb{E}\{ a_y ^2\} + 2\mathbb{E}\{ a_x ^4 a_y ^2\} - \mathbb{E}\{ a_x ^2\}\mathbb{E}\{ a_y ^4\} + 4\mathbb{E}\{ a_x ^2\}\mathbb{E}^2\{ a_y ^2\} + 8\mathbb{E}^2\{ a_x ^2\}\mathbb{E}\{ a_y ^2\}$ $+ 18\mathbb{E}\{ a_x ^2\} \mathbb{E}\{a_x^2\} ^2 - \mathbb{E}\{a_x^2\} ^2 - 9 \mathbb{E}\{a_x a_x ^2\} ^2 + 2\mathbb{E}\{ a_x ^2\} \mathbb{E}\{a_x^2\} ^2 - 4 \mathbb{E}\{a_x a_y ^2\} ^2 - 8 \mathbb{E}\{a_x a_y ^2\} ^2$ $+ 8 \mathbb{E}\{a_x a_y^*}\} ^2 \mathbb{E}\{ a_y ^2\} + 8 \mathbb{E}\{a_x a_y}\} ^2 \mathbb{E}\{ a_y ^2\} - \mathbb{E}\{a_x a_y^*}\} ^2 - \mathbb{E}\{a_x^* a_y^2\} ^2 + 16\mathbb{E}\{ a_x ^2\} \mathbb{E}\{a_x a_y^*}\} ^2$ $- 2 \mathbb{E}\{a_x^2 a_y^*}\} ^2 + 16\mathbb{E}\{ a_x ^2\} \mathbb{E}\{a_x a_y}\} ^2 + 4 \mathbb{E}\{a_x^2\} ^2 \mathbb{E}\{ a_y ^2\} - 2 \mathbb{E}\{a_x^2 a_y}\} ^2 + 2\Re\{4\mathbb{E}\{a_x a_y}\mathbb{E}\{a_x^* a_y}\}\mathbb{E}^*\{a_y^2\}$ $- 3\mathbb{E}\{a_x^2 a_x ^2\}\mathbb{E}^*\{a_x^2\} - 2\mathbb{E}\{ a_x ^2 a_y}\mathbb{E}\{a_y^* a_y ^2\} - \mathbb{E}\{ a_x ^2 a_y^2\}\mathbb{E}^*\{a_y^2\} - 2\mathbb{E}\{a_x a_y}\mathbb{E}^*\{a_x a_y a_y ^2\}$ $- \mathbb{E}\{a_x a_y^*}\mathbb{E}\{a_x^* a_y a_y ^2\} - 2\mathbb{E}\{a_x^2\}\mathbb{E}^*\{a_x^2 a_y ^2\} - \mathbb{E}\{a_x a_x ^2\}\mathbb{E}\{a_x a_y ^2\} - 4\mathbb{E}\{a_x a_y^*}\mathbb{E}\{a_x^* a_y a_x^2\}$ $- 4\mathbb{E}\{a_x a_y}\mathbb{E}^*\{a_x a_y a_x ^2\} + 8\mathbb{E}\{a_x^2\}\mathbb{E}^*\{a_x a_y}\mathbb{E}\{a_x^* a_y}\}\}$	✓		
Φ_4	$4\mathbb{E}\{ a_x ^2\}\mathbb{E}^2\{ b_x ^2\} + \mathbb{E}\{ a_y ^2\}\mathbb{E}\{ b_x ^2\}\mathbb{E}\{ b_y ^2\} + 4\mathbb{E}\{ a_x ^2\} \mathbb{E}\{b_x^* b_y}\} ^2 + \mathbb{E}\{ a_x ^2\}\mathbb{E}^2\{ b_y ^2\}$ $+ 2\Re\{2\mathbb{E}\{a_x a_y^*}\mathbb{E}\{ b_x ^2\}\mathbb{E}\{b_x^* b_y}\} + \mathbb{E}\{a_x a_y^*}\mathbb{E}\{ b_y ^2\}\mathbb{E}\{b_x^* b_y}\}\}$		✓	✓
Φ_5	$4\mathbb{E}\{ a_x ^2\} \mathbb{E}\{b_x b_y}\} ^2 + \mathbb{E}\{ a_y ^2\} \mathbb{E}\{b_x b_y}\} ^2 + 4\mathbb{E}\{ a_x ^2\} \mathbb{E}\{b_x^2\} ^2 + \mathbb{E}\{ a_x ^2\} \mathbb{E}\{b_y^2\} ^2$ $+ 2\Re\{2\mathbb{E}\{a_x a_y^*}\mathbb{E}^*\{b_x^2\}\mathbb{E}\{b_x b_y}\} + \mathbb{E}\{a_x a_y^*}\mathbb{E}\{b_y^2\}\mathbb{E}^*\{b_x b_y}\}\}$		✓	✓
Φ_6	$4\mathbb{E}\{ a_x ^2\}\mathbb{E}\{ b_x ^4\} - 8\mathbb{E}\{ a_x ^2\}\mathbb{E}^2\{ b_x ^2\} - 4\mathbb{E}\{ a_x ^2\} \mathbb{E}\{b_x^2\} ^2 - \mathbb{E}\{ a_y ^2\} \mathbb{E}\{b_x b_y^*}\} ^2 - \mathbb{E}\{ a_y ^2\} \mathbb{E}\{b_x b_y}\} ^2$ $+ \mathbb{E}\{ a_x ^2\}\mathbb{E}\{ b_y ^4\} - 2\mathbb{E}\{ a_x ^2\}\mathbb{E}^2\{ b_y ^2\} - \mathbb{E}\{ a_x ^2\} \mathbb{E}\{b_y^2\} ^2 - 2\mathbb{E}\{ a_x ^2\} \mathbb{E}\{b_x^* b_y}\} ^2 - 2\mathbb{E}\{ a_x ^2\} \mathbb{E}\{b_x b_y^*}\} ^2$ $- 4\mathbb{E}\{ a_x ^2\} \mathbb{E}\{b_x b_y}\} ^2 + 4\mathbb{E}\{ a_x ^2\}\mathbb{E}\{ b_x ^2 b_y ^2\} + \mathbb{E}\{ a_y ^2\}\mathbb{E}\{ b_x ^2 b_y ^2\} - 4\mathbb{E}\{ a_x ^2\}\mathbb{E}\{ b_x ^2\}\mathbb{E}\{ b_y ^2\}$ $- \mathbb{E}\{ a_y ^2\}\mathbb{E}\{ b_x ^2\}\mathbb{E}\{ b_y ^2\} + 2\Re\{-2\mathbb{E}\{a_x a_y^*}\mathbb{E}\{b_x b_y}\}\mathbb{E}^*\{b_x^2\} - \mathbb{E}\{a_x a_y^*}\mathbb{E}\{b_y^2\}\mathbb{E}^*\{b_x b_y}\}$ $- 2\mathbb{E}\{a_x a_y^*}\mathbb{E}\{ b_x ^2\}\mathbb{E}\{b_x^* b_y}\} - \mathbb{E}\{a_x a_y^*}\mathbb{E}\{ b_y ^2\}\mathbb{E}\{b_x^* b_y}\}\}$		✓	✓
Ψ_5	$4\mathbb{E}\{ b_x ^2\}\mathbb{E}^2\{ a_x ^2\} + 4\mathbb{E}\{ b_x ^2\} \mathbb{E}\{a_x^* a_y}\} ^2 + \mathbb{E}\{ b_y ^2\}\mathbb{E}\{ a_x ^2\}\mathbb{E}\{ a_y ^2\} + \mathbb{E}\{ b_x ^2\}\mathbb{E}^2\{ a_y ^2\}$ $+ 2\Re\{2\mathbb{E}\{b_x b_y^*}\mathbb{E}\{ a_x ^2\}\mathbb{E}\{a_x^* a_y}\} + \mathbb{E}\{b_x b_y^*}\mathbb{E}\{ a_y ^2\}\mathbb{E}\{a_x^* a_y}\}\}$		✓	✓
Ψ_6	$4\mathbb{E}\{ b_x ^2\} \mathbb{E}\{a_x^2\} ^2 + 4\mathbb{E}\{ b_x ^2\} \mathbb{E}\{a_x a_y}\} ^2 + \mathbb{E}\{ b_y ^2\} \mathbb{E}\{a_x a_y}\} ^2 + \mathbb{E}\{ b_x ^2\} \mathbb{E}\{a_y^2\} ^2$ $+ 2\Re\{2\mathbb{E}\{b_x b_y^*}\mathbb{E}^*\{a_x^2\}\mathbb{E}\{a_x a_y}\} + \mathbb{E}\{b_x b_y^*}\mathbb{E}\{a_y^2\}\mathbb{E}^*\{a_x a_y}\}\}$		✓	✓
Ψ_7	$4\mathbb{E}\{ b_x ^2\}\mathbb{E}\{ a_x ^4\} - 8\mathbb{E}\{ b_x ^2\}\mathbb{E}^2\{ a_x ^2\} - 4\mathbb{E}\{ b_x ^2\} \mathbb{E}\{a_x^2\} ^2 - \mathbb{E}\{ b_y ^2\} \mathbb{E}\{a_x a_y^*}\} ^2 - \mathbb{E}\{ b_y ^2\} \mathbb{E}\{a_x a_y}\} ^2$ $+ \mathbb{E}\{ b_x ^2\}\mathbb{E}\{ a_y ^4\} - 2\mathbb{E}\{ b_x ^2\}\mathbb{E}^2\{ a_y ^2\} - \mathbb{E}\{ b_x ^2\} \mathbb{E}\{a_y^2\} ^2 - 2\mathbb{E}\{ b_x ^2\} \mathbb{E}\{a_x^* a_y}\} ^2 - 2\mathbb{E}\{ b_x ^2\} \mathbb{E}\{a_x a_y^*}\} ^2$ $- 4\mathbb{E}\{ b_x ^2\} \mathbb{E}\{a_x a_y}\} ^2 + 4\mathbb{E}\{ b_x ^2\}\mathbb{E}\{ a_x ^2 a_y ^2\} + \mathbb{E}\{ b_y ^2\}\mathbb{E}\{ a_x ^2 a_y ^2\} - 4\mathbb{E}\{ b_x ^2\}\mathbb{E}\{ a_x ^2\}\mathbb{E}\{ a_y ^2\}$ $- 4\mathbb{E}\{ b_y ^2\}\mathbb{E}\{ a_x ^2\}\mathbb{E}\{ a_y ^2\} + 2\Re\{-2\mathbb{E}\{b_x b_y^*}\mathbb{E}\{a_x a_y}\}\mathbb{E}^*\{a_x^2\} - 2\mathbb{E}\{b_x b_y^*}\mathbb{E}\{ a_x ^2\}\mathbb{E}\{a_x^* a_y}\}$ $- \mathbb{E}\{b_x b_y^*}\mathbb{E}\{ a_y ^2\}\mathbb{E}\{a_x^* a_y}\} - \mathbb{E}\{b_x b_y^*}\mathbb{E}\{a_y^2\}\mathbb{E}^*\{a_x a_y}\}\}$		✓	✓
Λ_7	$\mathbb{E}\{ b_x ^2\}\mathbb{E}^2\{ a_x ^2\} + \mathbb{E}\{ b_y ^2\}\mathbb{E}\{ a_x ^2\}\mathbb{E}\{ a_y ^2\} + 2\Re\{\mathbb{E}\{b_x^* b_y}\mathbb{E}\{ a_x ^2\}\mathbb{E}\{a_x a_y^*}\}\}$		✓	✓
Λ_8	$\mathbb{E}\{ b_x ^2\}\mathbb{E}^2\{ a_x ^2\} + \mathbb{E}\{ b_y ^2\} \mathbb{E}\{a_x^* a_y}\} ^2 + 2\Re\{\mathbb{E}\{b_x^* b_y}\mathbb{E}\{ a_x ^2\}\mathbb{E}\{a_x a_y^*}\}\}$		✓	✓
Λ_9	$\mathbb{E}\{ b_x ^2\}\mathbb{E}\{ a_x ^4\} - 2\mathbb{E}\{ b_x ^2\}\mathbb{E}^2\{ a_x ^2\} - \mathbb{E}\{ b_x ^2\} \mathbb{E}\{a_x^2\} ^2 - \mathbb{E}\{ b_y ^2\} \mathbb{E}\{a_x a_y}\} ^2 - \mathbb{E}\{ b_y ^2\} \mathbb{E}\{a_x^* a_y}\} ^2$ $+ \mathbb{E}\{ b_y ^2\}\mathbb{E}\{ a_x ^2 a_y ^2\} - \mathbb{E}\{ b_y ^2\}\mathbb{E}\{ a_x ^2\}\mathbb{E}\{ a_y ^2\} + 2\Re\{-\mathbb{E}\{b_x^* b_y}\mathbb{E}\{a_x^2\}\mathbb{E}^*\{a_x a_y}\} - \mathbb{E}\{b_x^* b_y}\mathbb{E}\{ a_x ^2\}\mathbb{E}\{a_x a_y^*}\}\}$		✓	✓

TABLE III
EXPRESSION FOR THE TERMS USED IN (11) AND (12)

Term	Expression	SCI	XCI	MCI
χ_1	$\int_{-R_s/2}^{R_s/2} \int_{-R_s/2}^{R_s/2} P(f_1) ^2 P(f_2) ^2 P(f - f_1 + f_2) ^2 \mu(f_1, f_2, f) df_1 df_2$	✓	✓	
χ_2	$\int_{-R_s/2}^{R_s/2} \int_{-R_s/2}^{R_s/2} P(f_1) ^2 P(f_2) ^2 P(f - f_1 + f_2) ^2 \mu(f_1, f_2, f) \mu(f_1, f_1 - f_2 - f, f) df_1 df_2$	✓	✓	
χ_3	$ P(f) ^2 \int_{-R_s/2}^{R_s/2} \int_{-R_s/2}^{R_s/2} P(f_1) ^2 P(f_2) ^2 \mu(f_1, -f, f) \mu^*(f_2, -f, f) df_1 df_2$	✓		
χ_4	$\int_{-R_s/2}^{R_s/2} \int_{-R_s/2}^{R_s/2} \int_{-R_s/2}^{R_s/2} P(f_1) P^*(f_2) P(f - f_1 + f_2) P^*(f_1 - f_2) P(f_3) P^*(f - f_1 + f_2 + f_3) \mu(f_1, f_2, f) \cdot \mu^*(f_1 - f_2, f_3, f) df_1 df_2 df_3$	✓		
χ_5	$\int_{-R_s/2}^{R_s/2} \int_{-R_s/2}^{R_s/2} \int_{-R_s/2}^{R_s/2} P(f_1) P^*(f_2) P(f - f_1 + f_2) P(f_2 - f_1) P^*(f_3) P^*(f - f_1 + f_2 - f_3) \cdot \mu(f_1, f_2, f) \mu^*(f_3, f_2 - f_1, f) df_1 df_2 df_3$	✓		
χ_6	$\int_{-R_s/2}^{R_s/2} \int_{-R_s/2}^{R_s/2} \int_{-R_s/2}^{R_s/2} P(f_1) P^*(f_2) P(f - f_1 + f_2) P^*(f + f_2) P^*(f_3) P(f_2 + f_3) \mu(f_1, f_2, f) \cdot \mu^*(f_3, -f - f_2, f) df_1 df_2 df_3$	✓		
χ_7	$P(f) \int_{-R_s/2}^{R_s/2} \int_{-R_s/2}^{R_s/2} \int_{-R_s/2}^{R_s/2} P(f_1) ^2 P^*(f_2) P(f_3) P^*(f - f_2 + f_3) \mu(f_1, -f, f) \mu^*(f_2, f_3, f) df_1 df_2 df_3$	✓		
χ_8	$\int_{-R_s/2}^{R_s/2} \int_{-R_s/2}^{R_s/2} \int_{-R_s/2}^{R_s/2} P(f_1) ^2 P^*(f_2) P(f - f_1 + f_2) P(f_3) P^*(f - f_1 + f_3) \mu(f_1, f_2, f) \mu^*(f_1, f_3, f) df_1 df_2 df_3$	✓		
χ_9	$\int_{-R_s/2}^{R_s/2} \int_{-R_s/2}^{R_s/2} \int_{-R_s/2}^{R_s/2} P(f_1) ^2 P^*(f_2) P(f - f_1 + f_2) P^*(f_3) P^*(f - f_1 - f_3) \mu(f_1, f_2, f) \mu^*(f_3, -f_1, f) df_1 df_2 df_3$	✓		
χ_{10}	$\int_{-R_s/2}^{R_s/2} \int_{-R_s/2}^{R_s/2} \int_{-R_s/2}^{R_s/2} P(f_1) P(f_2) ^2 P(f - f_1 + f_2) P^*(f_3) P^*(f + f_2 - f_3) \mu(f_1, f_2, f) \mu^*(f_3, f_2, f) df_1 df_2 df_3$	✓	✓	
χ_{11}	$\int_{-R_s/2}^{R_s/2} \int_{-R_s/2}^{R_s/2} \int_{-R_s/2}^{R_s/2} P(f_1) P^*(f_2) P(f - f_1 + f_2) P^*(f_3) P(f_4) P^*(f - f_3 + f_4) \cdot \mu(f_1, f_2, f) \mu^*(f_3, f_4, f) df_1 df_2 df_3 df_4$	✓		
χ_{12}	$\int_{-R_s/2}^{R_s/2} \int_{f_c - R_s/2}^{f_c + R_s/2} P(f_1) ^2 P(f_2) ^2 P(f - f_1 + f_2) ^2 \mu(f_1, f_2, f) df_1 df_2$		✓	
χ_{13}	$\int_{-R_s/2}^{R_s/2} \int_{f_c - R_s/2}^{f_c + R_s/2} P(f_1) ^2 P(f_2) ^2 P^*(f - f_1 - f_2 + 2f_c) P(f - f_1 + f_2) P^*(2f_c - f_2) \mu(f_1, f_2, f) \cdot \mu^*(f_1, f_1 - f_2 - f + 2f_c, f) df_1 df_2$		✓	
χ_{14}	$\int_{-R_s/2}^{R_s/2} \int_{f_c - R_s/2}^{f_c + R_s/2} \int_{f_c - R_s/2}^{f_c + R_s/2} P(f_1) ^2 P(f_2) ^2 P(f_3) ^2 P(f - f_1 + f_2) P^*(f - f_1 + f_3) \mu(f_1, f_2, f) \mu^*(f_1, f_3, f) df_1 df_2 df_3$		✓	
χ_{15}	$\int_{-R_s/2}^{R_s/2} \int_{f_c - R_s/2}^{f_c + R_s/2} P(f_1) ^2 P(f_2) ^2 P^*(f_1 - f_2 - f + f_c) P(f - f_1 + f_2) ^2 \mu(f_1, f_2, f) \mu^*(f_1, f_1 - f_2 - f + f_c, f) df_1 df_2$		✓	
χ_{16}	$\int_{f_c - R_s/2}^{f_c + R_s/2} \int_{n f_c - R_s/2}^{n f_c + R_s/2} P(f_1) ^2 P(f_2) ^2 P(f - f_1 + f_2) ^2 \mu(f_1, f_2, f) df_1 df_2$ (with $n \in M1$)			✓
χ_{17}	$\int_{f_c - R_s/2}^{f_c + R_s/2} \int_{n f_c - R_s/2}^{n f_c + R_s/2} P(f_1) ^2 P(f_2) ^2 P^*(f - f_1 - f_2 + 2f_c) P(f - f_1 + f_2) P^*(2f_c - f_2) \mu(f_1, f_2, f) \cdot \mu^*(f_1, f_1 - f_2 - f + 2f_c, f) df_1 df_2$ (with $n \in M1$)			✓
χ_{18}	$\int_{f_c - R_s/2}^{f_c + R_s/2} \int_{n f_c - R_s/2}^{n f_c + R_s/2} \int_{n f_c - R_s/2}^{n f_c + R_s/2} P(f_1) ^2 P(f_2) ^2 P^*(f_3) P(f - f_1 + f_2) P^*(f - f_1 + f_3) \cdot \mu(f_1, f_2, f) \mu^*(f_1, f_3, f) df_1 df_2 df_3$ (with $n \in M1$)			✓
χ_{19}	$\int_{f_c - R_s/2}^{f_c + R_s/2} \int_{n f_c - R_s/2}^{n f_c + R_s/2} P(f_1) ^2 P(f_2) ^2 P(f - f_1 + f_2) ^2 \mu(f_1, f_2, f) df_1 df_2$ (with $n \in M2$)			✓
χ_{20}	$\int_{f_c - R_s/2}^{f_c + R_s/2} \int_{n f_c - R_s/2}^{n f_c + R_s/2} P(f_1) ^2 P(f_2) ^2 P^*(f_1 - f_2 - f + f_c) P(f - f_1 + f_2) ^2 \cdot \mu(f_1, f_2, f) \mu^*(f_1, f_1 - f_2 - f + f_c, f) df_1 df_2$ (with $n \in M2$)			✓
χ_{21}	$\int_{f_c - R_s/2}^{f_c + R_s/2} \int_{n f_c - R_s/2}^{n f_c + R_s/2} \int_{n f_c - R_s/2}^{n f_c + R_s/2} P(f_1) ^2 P(f_2) ^2 P^*(f_3) P(f - f_1 + f_2) P^*(f - f_1 + f_3) \cdot \mu(f_1, f_2, f) \mu^*(f_1, f_3, f) df_1 df_2 df_3$ (with $n \in M2$)			✓
χ_{22}	$\int_{n f_c - R_s/2}^{n f_c + R_s/2} \int_{n f_c - R_s/2}^{n f_c + R_s/2} P(f_1) ^2 P(f_2) ^2 P(f - f_1 + f_2) ^2 \mu(f_1, f_2, f) df_1 df_2$ (with $n \in M3$)			✓
χ_{23}	$\int_{n f_c - R_s/2}^{n f_c + R_s/2} \int_{n f_c - R_s/2}^{n f_c + R_s/2} P(f_1) ^2 P(f_2) ^2 P(f - f_1 + f_2) ^2 \mu(f_1, f_2, f) \mu(f_1, f_1 - f_2 - f, f) df_1 df_2$ (with $n \in M3$)			✓
χ_{24}	$\int_{n f_c - R_s/2}^{n f_c + R_s/2} \int_{n f_c - R_s/2}^{n f_c + R_s/2} \int_{n f_c - R_s/2}^{n f_c + R_s/2} P(f_1) P(f_2) ^2 P(f - f_1 + f_2) P^*(f_3) P^*(f + f_2 - f_3) \cdot \mu(f_1, f_2, f) \mu^*(f_3, f_2, f) df_1 df_2 df_3$ (with $n \in M3$)			✓

The value range of n (i.e., M1, M2 and M3) is shown in Appendix. B.

In Theorem 1, the coefficients $\Phi_k, \Psi_k, \Lambda_k, k = 4, 5, \dots, 9$ in (12) represent modulation-dependent intra- and cross-polarization moments of the DP-4D modulation formats. The terms $\chi_k, k = 12, 13, \dots, 15$ are integrals related to the channel parameters. In addition, the XCI power coefficient can be obtained by summing the x and y components, i.e., $\eta_{ss, XCI} = \eta_{ss, XCI}^x + \eta_{ss, XCI}^y$ where the $\eta_{ss, XCI}^y$ can be obtained from (12) by swapping the polarization labels $x \rightarrow y$ and $y \rightarrow x$. Note that (12) is valid under the following assumptions:

- the sequence of DP-4D transmitted symbols \mathbf{a}_n for $n \in \mathbb{Z}$ are statistically independent,
- the transmitted pulse $p(t)$ has a rectangular (or quasi-rectangular) spectrum, and
- a first-order RP framework for the solution of the Manakov equation.

C. MCI contribution

Generally, MCI is always thought as weaker than SCI and XCI, especially in high dispersion fibers, as investigated in [39]. This is due to the fact that the higher the dispersion, the faster is the (amplitude) decay of the link function $\mu(f_1, f_2, f)$ (see (18), ahead) away from its maximum. Conversely, the lower the dispersion, the slower the decay. Therefore, to accurately predict the nonlinear interference in various scenarios, the MCI contribution was derived following an approach similar to [37, Appendix D].

As shown in Fig. 2, the MCI can be divided into four contributions corresponding to the integration islands marked as M0, M1, M2 and M3. The M1 and M2 (yellow and red) regions have a similar structure as XCI in the region X1 (blue), and M3 (green) is similar to the region X3 (purple). Taking the M1 in the domains locating in the second quadrant, parallel

to f_2 as an example, the triples of M1 can be shown as $(f_{\text{INT},1}, f_{\text{INT},-1}, f_{\text{INT},-1})$ and the triples of X1 can be shown as $(f_{\text{COI}}, f_{\text{INT},1}, f_{\text{INT},1})$. If the $(f_{\text{INT},1})$ is regarded as (f_{COI}) , M1 has the similar structure of X1. Thus, (12) can be used to approximate the contributions of M1, M2 and M3 islands, where the only difference is the integration limits. In particular, for the M0 island, we take the same approach in [37], i.e., the contribution of M0 island is produced entirely according to the GN-model, denoted as $\bar{\eta}_{\text{M0}}^x$. The following theorem gives the MCI contributions.

Theorem 2: If all channels are assumed to have the same transmitted power and the total number of channel N_{ch} is odd, the $\eta_{\text{ss,MCI}} = \eta_{\text{ss,MCI}}^x + \eta_{\text{ss,MCI}}^y$ is similar to (12), which can be expressed as

$$\begin{aligned} \eta_{\text{ss,MCI}}^x = & 2 \cdot \left(\frac{8}{9}\right)^2 \frac{\gamma^2}{P^3} \left[R_s^3 [\Phi_4(\chi_{16} + \chi_{19}) + \Phi_5(\chi_{17} + \chi_{20}) \right. \\ & + \Lambda_7 \chi_{22} + \Lambda_8 \chi_{23}] + R_s^2 [\Phi_6(\chi_{18} + \chi_{21}) \\ & \left. + \Lambda_9 \chi_{24}] \right] + \bar{\eta}_{\text{M0}}^x, \end{aligned} \quad (13)$$

where the terms $\Phi_k, \Lambda_k, k = 4, 5, \dots, 9$ are same with the (12) and shown in Table II. The terms $\chi_k, k = 16, 17, \dots, 24$ are shown in Table III.

Theorem 2 shows the MCI power coefficient for the x component. By swapping the polarization labels $x \rightarrow y$ and $y \rightarrow x$, $\eta_{\text{ss,XCI}}^y$ can be obtained. A detailed explanation of the integration regions for M1, M2 and M3 is shown in Appendix B.

IV. SIMULATION RESULTS AND ANALYSIS

The numerical validation of the model in this work is performed via SSFM simulations, where the optical nonlinearity is kept as the only noise. The simulated multi-span optical system is described in Table IV. To verify the reliability of our proposed model, various 4D modulation formats are considered in our simulations. Some of these formats are taken from the sphere packing database in [40], and some from recently proposed 4D symmetric formats (such as 4D-PRS64 [14] and a family of 4D orthant-symmetric (OS) formats [41]). Finally, nonsymmetric modulation formats such as the so-called c4_16 [42] and w4_64 [4] are also considered.³

In this section, we compared 4D modulation formats in terms of η_{ss} to verify the accuracy of the proposed model. To validate the η_{ss} value, SSFM does not consider the ASE noise, i.e., the ideal EDFA compensates fiber loss without adding optical noise. In the absence of other noise sources, $\eta_{\text{ss}} = \eta_{\text{ss,x}} + \eta_{\text{ss,y}}$ can be estimated via the received SNR for COI via the relationship

$$\eta_{\text{ss,x}} \approx \frac{P_x}{\text{SNR}_{\text{eff,x}}^{\text{SSFM}} P^3}, \quad (14)$$

³The coordinates and labeling of all the 4D modulation formats used in this paper can be found online at <https://github.com/TUe-ICTLab/Binary-Labeling-for-2D-and-4D-constellations>.

TABLE IV
SYSTEM AND FIBER PARAMETERS

	Parameter	Value
TX parameters	Symbol rate (R_s)	45 GBaud
	No. of channels	1 (Figs. 5, 6(a)) 9 (Figs. 3, 4, 6(b))
	RRC rolloff	0.01%
	Tx Power (P)	-20 dBm (Figs. 3-4)
Link parameters	Span length	80 km
	No. of spans	20 (Fig. 4)
SMF (Figs. 5, 3 - 6)	Attenuation coeff. (α)	0.2 dB/km
	Dispersion par. (D)	17 ps/nm/km
	Nonlinear coeff. (γ)	$1.3 (\text{W} \cdot \text{km})^{-1}$
NZDSF (Figs. 3)	Attenuation coeff. (α)	0.2 dB/km
	Dispersion par. (D)	3.8 ps/nm/km
	Nonlinear coeff. (γ)	$1.5 (\text{W} \cdot \text{km})^{-1}$
LDF (Figs. 3)	Attenuation coeff. (α)	0.2 dB/km
	Dispersion par. (D)	-1.8 ps/nm/km
	Nonlinear coeff. (γ)	$2.2 (\text{W} \cdot \text{km})^{-1}$
SSFM parameters	Step size	0.1 km
	Samples per symbol	4
	Noise figure	5 dB

where P_x and $\text{SNR}_{\text{eff,x}}^{\text{SSFM}}$ are the transmitted power and the effective SNR over the x polarization, respectively. The value of $\text{SNR}_{\text{eff,x}}^{\text{SSFM}}$ is estimated via [28, eq. (22)]

$$\text{SNR}_{\text{eff,x}}^{\text{SSFM}} = \frac{\sum_{j=1}^M |\bar{y}_j|^2}{\sum_{j=1}^M \mathbb{E}\{|Y - \bar{y}_j|^2 | X = x_j\}}, \quad (15)$$

in which the X and Y are RVs representing the transmitted symbols and received symbols over x polarisation, respectively. In (15), M is the number of constellation points and x_j represents the j -th constellation point. The variable \bar{y}_j represents conditional mean, i.e., $\bar{y}_j = \mathbb{E}\{Y | X = x_j\}$, where $\mathbb{E}\{\cdot\}$ is the statistical expectation.

The NLI models we consider in this paper were derived under a perturbation theory framework. These NLI models are then used to predict optical communication system performance in the linear and pseudo-linear regimes. Thus, all channels used a flat launch power of $P = -20$ dBm. Note that η_{ss} is a function of several system parameters, albeit independent of the transmitted power.

A. Numerical Validation for Multi-Channel Transmission

In this subsection, we show the NLI power coefficient versus the number of spans for transmitting the nonsymmetric constellation voronoi4_32 [5] in three different fiber types, i.e., standard SMF, non-zero dispersion-shifted fiber (NZDSF), low dispersion fiber (LDF), which are listed in Table IV. To remove SCI, we ran a single-channel simulation and recorded its NLI power coefficient $\eta_{\text{ss,SCI}}$. By subtracting $\eta_{\text{ss,SCI}}$ in total NLI power coefficient η_{ss} of WDM simulations, the residual coefficient was estimated as $\eta_{\text{ss,XMCI}}$ [43].

In Fig. 3, the $\eta_{\text{ss,XPM}}$ is approximately equal to $\eta_{\text{ss,X1}}$ in (34), shown as a green solid line. The blue solid line represents $\eta_{\text{ss,XCI}}$ given by (12). The marks represent the simulation results which account for all NLI except SCI. Fig. 3 (a) shows that the XCI or XPM is sufficient to present simulated NLI (except SCI) over high accumulated dispersion scenarios

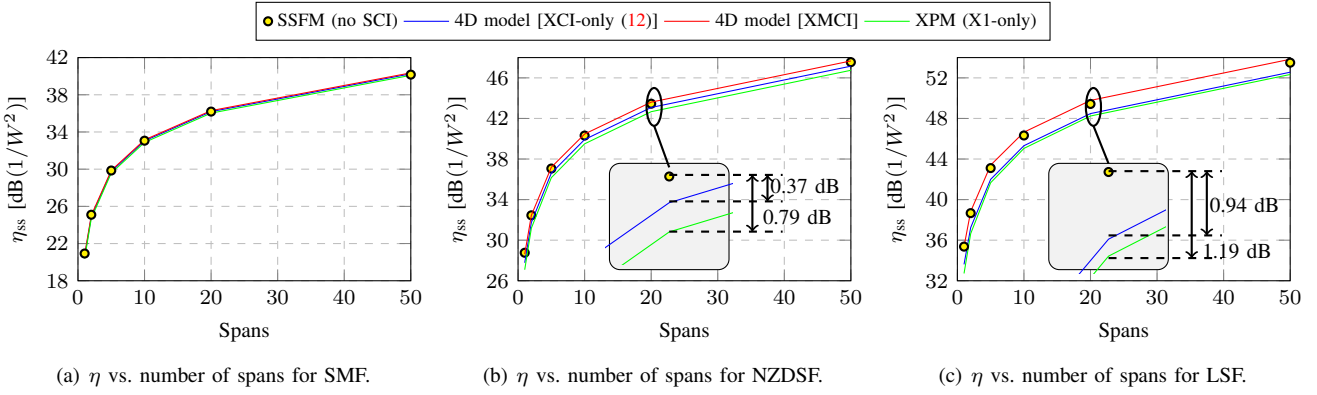


Fig. 3. Simulation results of multi-span 9-channel optical fiber transmission system for three fiber types: (a) SMF, (b) NZDSF and (c) LDF. The nonsymmetric constellation voronoi4_32 [5] was used for transmission. Blue solid line is $\eta_{ss,XCI}$ in (12). Red solid line is $\eta_{ss,XMCI}$ (i.e., XCI + MCI). Green solid line is the XPM $\eta_{ss,XPM}$, which is approximately equal to $\eta_{ss,X1}$ in (34). The marks are SSFM simulations with single-channel nonlinearity (SCI) removed.

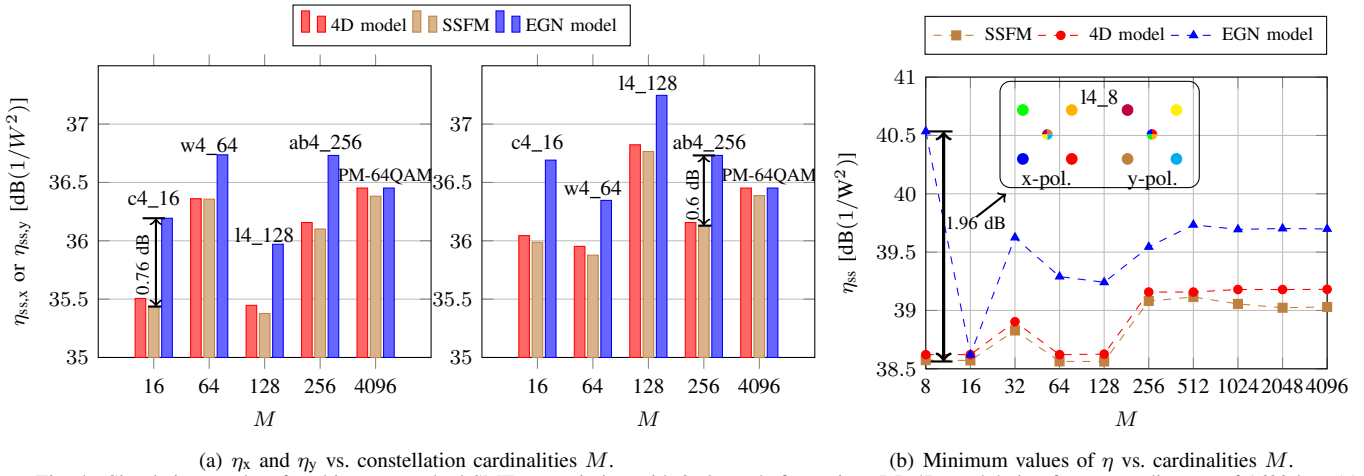


Fig. 4. Simulation results of multi-span standard SMF transmission with 9 channels for various DP-4D modulation formats at distance of 1600 km. (a) plots the NLI power coefficient η_x (left) and η_y (right) for different constellation cardinalities M : the red bar is the 4D model (including SCI, XCI and MCI), the brown bar is SSFM; the blue bar is EGN model [25], respectively. (b) plots minimum values of η vs. different constellation cardinalities M : the blue dashed line is EGN model; the red dashed is 4D model; the brown dashed line is SSFM.

for example standard SMF fiber. According to the inset of Fig. 3 (b), the XPM underestimate the simulated NLI by about 0.79 dB, while the XCI can reduce such error to 0.37 dB. And the inset of Fig. 3 (c) considered a ultra-low dispersion fiber, showing a wide underestimate error of about 1.19 dB for XPM and 0.94 dB for XCI. While as shown the red solid line which represents $\eta_{ss,XMCI} = \eta_{ss,XCI} + \eta_{ss,MCI}$, the 4D model with MCI under consideration matches well with the SSFM results for all the three considered fibers including the low and ultra-low dispersion fibers. This suggests that the XCI-only or XPM can not represent all NLI (except SCI), especially in low accumulated dispersion scenarios.

In Fig. 4 (a), the values of $\eta_{ss,x}$ (left) and $\eta_{ss,y}$ (right) were estimated using different models for 16-point, 64-point, 128-point, 256-point and 4096-point constellations. We considered (i) the proposed 4D model including SCI, XCI and MCI (red bars), (ii) the EGN model (blue bars), and (iii) SSFM results (brown bars). For PM-2D modulation formats such as PM-64QAM, our model gives the same result as the EGN model and approximate quite well the SSFM results. For nonsymmetric constellations, the EGN model leads to

inaccuracies of up to 0.76 dB for $\eta_{ss,x}$ for “c4_16” [42]. Even for symmetric constellations, the EGN model also leads to inaccuracies of up to 0.60 dB for $\eta_{ss,y}$ in “ab4_256” [44]. Such errors between the EGN model results and the SSFM results indicate obvious limitations of the EGN model in predicting the NLI of 4D modulation formats. For all constellations shown, the 4D model has ability to predict NLI of DP-4D modulation formats within acceptable margin of error (< 0.07 dB).

To further validate our proposed 4D model, more 4D modulation formats with different constellation cardinalities against the NLI power coefficient η_{ss} were investigated in Fig. 4. Among these, the minimum values of the NLI power coefficient η_{ss} are shown in Fig. 4 (b) for each M . The corresponding values are also listed in Table V for x- and y- polarization. For all constellations shown, the EGN model overestimates the value of the NLI power coefficient η_{ss} with deviations up to 1.96 dB ($M=8$: 14_8). The reason is discussed in detail in next paragraph. Conversely, the 4D model is in perfect agreement with the simulation results with the maximum only deviation about 0.15 dB (for all constellation

TABLE V
 η -OPTIMAL FORMATS IN FIG. 4 (B)

Const. label	M	$(\eta_{ss,x}, \eta_{ss,y})$ [dB $1/W^2$]
l4_8	8	(35.6, 35.6)
cube4_16	16	(35.6, 35.6)
b4_32	32	(35.9, 35.9)
4D-PRS64	64	(35.6, 35.6)
4D-2A-8PSK7b	128	(35.6, 36.6)
w4_256	256	(35.2, 35.2)
sphere_512	512	(36.2, 36.2)
a4_1024	1024	(36.2, 36.2)
a4_2048	2048	(36.1, 36.2)
a4_4096	4096	(36.3, 36.1)

cardinalities M).

It is known that all modulation-dependent coefficients $\Phi_k, k = 1, 2, \dots, 6, \Psi_k, k = 1, 2, \dots, 7, \Lambda_k, k = 1, 2, \dots, 9$, and Ξ_1 in (11), (12) and (13) can be divided into intra- and cross-polarization terms. For the EGN model, it is derived under the assumption that a_x and a_y are statistically independent and identically distributed, namely that most cross-polarization terms are neglected, for example $\mathbb{E}\{a_x a_y^*\} = 0$. That is reason that the EGN model always overestimates the NLI power coefficient as shown in Fig. 4. Interestingly, most of these cross-polarization terms are either zero or are small, except for these three terms $\mathbb{E}\{|a_x|^2 |a_y|^2\}$, $\mathbb{E}\{|a_x|^2 |a_y|^4\}$ and $\mathbb{E}\{|a_y|^2 |a_x|^4\}$. For the constellation of “l4_8”, the values of these three terms are equal to zero in 4D model and 0.25 in EGN model. On the other hand, the point at origin in the first 2D must transmitted in combination with a $\bullet/\bullet/\bullet/\bullet$ point in the second 2D as the inset in Fig 4 (b). Thus, the constellation of “l4_8” has the constant-modulus property so that it has better nonlinear tolerance.

B. Analysis in the presence of Signal-ASE Noise beating

The previous simulation results indicate that the proposed model would be accurate enough to predict the contribution of NLI in short links, where signal-signal noise interaction are predominant. In this section, the effect of signal-ASE noise interaction in the prediction of the effective SNR for general DP-4D modulation formats is evaluated via (9), including both of the signal-signal interaction and signal-ASE noise interaction.

Fig. 5 shows the noise powers $\sigma_{ASEtot}^2, \sigma_{ss}^2, \sigma_{sn}^2$ in (9), against transmission distance, for two modulation formats: PM-256QAM and 4D-PRS64 [14]. The system parameters are shown in Table IV. For all distance shown, the total ASE noise power is constellation-independent and the NLI contribution of signal-signal and signal-ASE interactions is smaller than the total ASE noise power. Comparing the solid and dashed lines, the dependency of the NLI noise on the modulation format is shown. A 0.3 dB gap can be observed when comparing these two modulation formats at 4000 km. In addition, when these two modulation formats are compared at a distance of 1600 km, σ_{sn}^2 differs from σ_{ss}^2 by 17.2 dB. This difference is reduced to 10.6 dB at 7500 km. The proportion of σ_{sn}^2 in NLI power keeps increasing as the number of fiber span increases. This indicates that the effect of signal-ASE noise NLI can not be fully neglected in long-distance transmission.

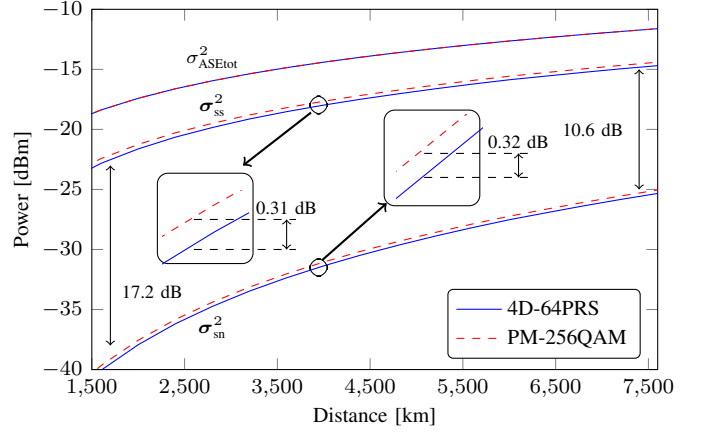
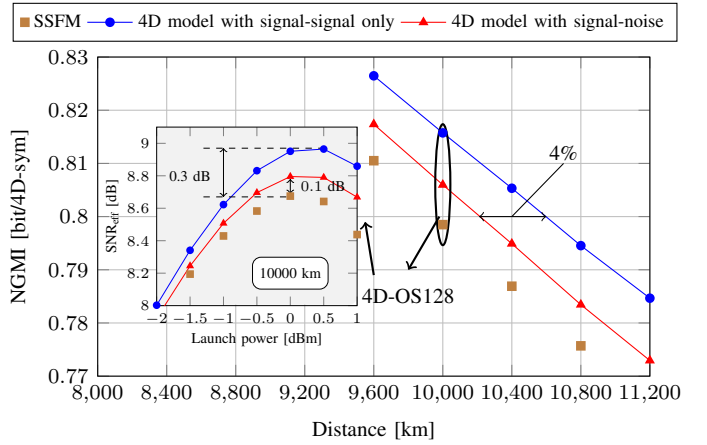
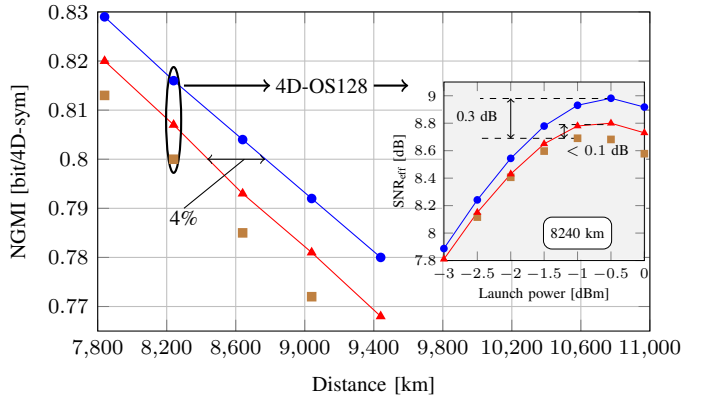


Fig. 5. Noise power versus transmission distance at launch power of $P = 0.5$ dBm with a single channel. Noise is shown separately, as total ASE noise, signal-signal NLI and signal-ASE noise NLI in (9).



(a) NGMI vs. transmission distance at optimal launch power for 4D-OS128 modulation format with a single-channel system. Inset: SNR_{eff} vs. launch power.



(b) NGMI vs. transmission distance at optimal launch power for 4D-OS128 modulation format with a multi-channel system. Inset: SNR_{eff} vs. launch power.

Fig. 6. Transmission performance using 4D-OS128 modulation format.

Fig. 6 shows the transmission performance estimation in terms of normalized generalized mutual information (NGMI) for the 4D model with signal-noise interactions, using the 4D-OS128 modulation format. In Fig. 6 (a) and (b), we can observe that the 4D model with signal-noise interactions can reduce the transmission reach prediction error by 4% relative to the 4D model with signal-signal interactions only, at NGMI

of 0.8 for both single-channel and multi-channel systems. The prediction accuracy gains come from the larger overestimated SNR_{eff} of 0.3 dB for the 4D model with signal-signal interactions only, compared to the SSFM results. As shown in the insets of Fig. 6 (a) and (b), the proposed 4D model with signal-noise interactions reduces the SNR deviation within 0.1 dB for both single-channel and multi-channel systems, compared to the 4D model with signal-signal interactions only. Therefore, the 4D model with signal-noise provides a better accuracy on performance prediction than 4D model with signal-signal interactions only, especially in long-distance transmission.

V. CONCLUSIONS

An “ultimate” 4D nonlinear interference model accounting for the intra- and inter-channel nonlinearity for the entire DP-4D class of modulation formats was proposed and validated in detail for multi-channel optical transmission systems. Unlike the EGN model, which ignores the inter-polarization dependencies, our model makes no assumptions on either the marginal or joint statistics of the two polarization components of the transmitted 4D modulation formats besides being zero mean. The proposed model has the ability to predict the SCI, XCI and MCI nonlinear terms—splitted into intra-polarization and cross-polarization terms—for arbitrary DP-4D modulation formats. In addition, the proposed model is shown to be accurate for various scenarios, including both high and low dispersion fiber systems. Comparing the induced NLI for different 4D modulation formats, the numerical results show that the EGN model overestimates the NLI power up to 1.96 dB, while the proposed 4D NLI model can reduce the NLI power estimation error within 0.15 dB from the SSFM simulation results.

On the other hand, we evaluated the weight of signal-ASE noise interaction in the prediction of the effective SNR of general DP-4D constellations. Our results show that when signal-ASE noise interactions are considered the accuracy of SNR estimation is improved by about 0.2 dB in single-channel or multi-channel WDM systems.

The proposed 4D NLI model in this work is a powerful analytical tool for the global optimization of 4D modulation formats in the optical fiber channel.

APPENDIX A PROOF OF THEOREM 1

To find an analytical expression for NLI power, firstly, a solution to the Manakov equation, which is the fundamental equation of dual-polarization fiber non-linear dispersive propagation, must be found. We start from the Manakov equation which can be written in time domain as [45]

$$\frac{\partial E(t, z)}{\partial z} = -\frac{\alpha}{2}E(t, z) - j\frac{\beta_2}{2}\frac{\partial^2 E(t, z)}{\partial t^2} + j\frac{8}{9}\gamma|E(t, z)|^2E(t, z), \quad (16)$$

where α is the loss coefficient, β_2 is dispersion coefficient and γ is the nonlinear coefficient. As it is well-known, the Manakov equation has no general closed-form solutions. Like most of the existing NLI power models in the literature [24], [25], [34], the model derived here operates within a

first-order perturbative framework. In particular, a frequency-domain first-order regular perturbation (RP) approach in the γ coefficient is performed [23], [46]. Therefore, the first order RP solution of the Manakov equation after N_s spans is expressed as [27, eq. (13)]

$$\begin{aligned} E(f, N_s, L_s) &= [E_x(f, N_s, L_s), E_y(f, N_s, L_s)]^T \\ &= -j\frac{8}{9}\gamma \int_{-\infty}^{\infty} \int_{-\infty}^{\infty} E^T(f_1, 0)E^*(f_2, 0) \\ &\quad E(f - f_1 + f_2, 0)\mu(f_1, f_2, f, N_s, L_s)df_1df_2. \end{aligned} \quad (17)$$

Due to the lumped amplification and identical spans assumption, $\mu(f_1, f_2, f, N_s, L_s)$ defined in [43, eq. 19] can be expressed as

$$\begin{aligned} \mu(f_1, f_2, f, N_s, L_s) &\triangleq \frac{1 - e^{-\alpha L_s} e^{j4\pi^2\beta_2(f-f_1)(f_2-f_1)L_s}}{\alpha - j4\pi^2\beta_2(f-f_1)(f_2-f_1)} \\ &\quad \cdot \sum_{l=1}^{N_s} e^{-j4\pi^2\beta_2(f-f_1)(f_2-f_1)L_s}. \end{aligned} \quad (18)$$

This formula called the “link function” is a function of the link parameters and not dependent on characteristics of the launched signal. As shown in this formula, the “link function” represents the contribution of different NLI fields (f_1, f_2, f) accumulated in different spans so that it weights the generation of NLI and relates to channel parameters.

Under the assumption that the transmitted signal model is periodic with period T , where W symbols are transmitted every period T , the WDM transmitted signal model can be expressed as (1) and (2) as shown in Sec. II. The Fourier transform of the $E(t, 0)$ is given by

$$E(f, 0) = \sqrt{\Delta_f} \sum_{h=1}^{N_{ch}} \sum_{k=-\infty}^{+\infty} \zeta_{k,h} \delta(f - f_c - k\Delta_f), \quad (19)$$

where $\Delta_f = 1/T$ and

$$\begin{aligned} \zeta_{k,h} &= [\zeta_{x,k,h}, \zeta_{y,k,h}]^T \\ &= \sqrt{\Delta_f} P(f_c + k\Delta_f) \sum_{n=-(W-1)/2}^{(W-1)/2} c_n e^{-j2\pi\frac{kn}{W}}, \end{aligned} \quad (20)$$

is the discrete Fourier transforms of the h -th channel transmitted symbol sequence $(\mathbf{a}_n$ or $\mathbf{b}_n)$.

Only considering a COI and an INT channel, the transmitted signal model can be simplified as

$$\begin{aligned} E(f, 0) &= \sqrt{\Delta_f} \sum_{k=-\infty}^{+\infty} \nu_k \delta(f - k\Delta_f) \\ &\quad + \sqrt{\Delta_f} \sum_{k=-\infty}^{+\infty} \xi_k \delta(f - f_c - k\Delta_f), \end{aligned} \quad (21)$$

where

$$\nu_k = [\nu_{x,k}, \nu_{y,k}]^T = \sqrt{\Delta_f} P(k\Delta_f) \sum_{n=-(W-1)/2}^{(W-1)/2} \mathbf{a}_n e^{-j2\pi\frac{kn}{W}},$$

and

$$\boldsymbol{\xi}_k = [\xi_{x,k}, \xi_{y,k}]^T = \sqrt{\Delta_f} P(f_c + k\Delta_f) \sum_{n=-(W-1)/2}^{(W-1)/2} \mathbf{b}_n e^{-j2\pi \frac{kn}{W}}.$$

in which $\mathbf{a}_n = [a_{x,n}, a_{y,n}]^T$ are random vectors transmitted by the COI, complex symbols modulated on two arbitrary orthogonal polarization states x and y , respectively. $\mathbf{b}_n = [b_{x,n}, b_{y,n}]^T$ is RVs transmitted by an INT channel.

Substituting the spectrum of the transmitted periodic signal (21) in (17), we obtain the PSD of received NLI for x component,

$$\begin{aligned} E_x(f, N_s, L_s) &= -j \frac{8}{9} \gamma \Delta_f^{3/2} \sum_{i=-\infty}^{\infty} \delta(f - i\Delta_f) \\ &\left[\sum_{S_i} (\nu_{x,k} \nu_{x,m}^* \nu_{x,n} + \nu_{y,k} \nu_{y,m}^* \nu_{x,n}) \mu(S_i, N_s, L_s) \right. \\ &+ \sum_{X1_i} (2\nu_{x,k} \xi_{x,m}^* \xi_{x,n} + \nu_{y,k} \xi_{y,m}^* \xi_{x,n} + \nu_{x,k} \xi_{y,m}^* \xi_{y,n}) \mu(X1_i, N_s, L_s) \\ &+ \sum_{X2_i} (2\nu_{x,k} \nu_{x,m}^* \xi_{x,n} + \nu_{y,k} \nu_{y,m}^* \xi_{x,n} + \nu_{x,k} \nu_{y,m}^* \xi_{y,n}) \mu(X2_i, N_s, L_s) \\ &+ \sum_{X3_i} (\nu_{x,k} \xi_{x,m}^* \nu_{x,n} + \nu_{y,k} \xi_{y,m}^* \nu_{x,n}) \mu(X3_i, N_s, L_s) \\ &+ \sum_{X4_i} (\xi_{x,k} \xi_{x,m}^* \xi_{x,n} + \xi_{y,k} \xi_{y,m}^* \xi_{x,n}) \mu(X4_i, N_s, L_s) \\ &\left. + \sum_{X5_i} (\xi_{x,k} \nu_{x,m}^* \xi_{x,n} + \xi_{y,k} \nu_{y,m}^* \xi_{x,n}) \mu(X5_i, N_s, L_s) \right], \end{aligned} \quad (22)$$

where

$$\begin{aligned} X1_i &= S_i = \{(k, m, n) : (k - m + n)\Delta_f = i\Delta_f\} \\ X2_i &= X4_i = \{(k, m, n) : (k - m + n)\Delta_f + f_c = i\Delta_f\} \\ X3_i &= \{(k, m, n) : (k - m + n)\Delta_f - f_c = i\Delta_f\} \\ X5_i &= \{(k, m, n) : (k - m + n)\Delta_f + 2f_c = i\Delta_f\}, \end{aligned}$$

are the integration regions.

The first summation S_i is SCI, which is dealt with in [27]. Note that the summation of $X5_i$ is always zero [37, Appendix C], when the channels do not overlap, i.e., the INT channel center frequency satisfies the relation of $f_c \geq R_s$.

The PSD of the first order NLI is defined as [27, eq. (20)]

$$\begin{aligned} \bar{S}(f, N_s, L_s) &= [\bar{S}_x(f, N_s, L_s), \bar{S}_y(f, N_s, L_s)]^T \\ &= [\mathbb{E}\{|E_x(f, N_s, L_s)|^2\}, \mathbb{E}\{|E_y(f, N_s, L_s)|^2\}], \end{aligned} \quad (23)$$

where $\mathbb{E}\{\cdot\}$ is the statistical expectation.

Substituting the expression (22) in (23), we obtain the PSD of received XCI. For the sake of brevity, we just present the detailed derivation of the set $X1_i$ for the x component. As for the field on the y polarization, it can be found by swapping the subscripts x and y , and the other set can be derived following the same approach.

For the region $X1_i$, we have

$$\begin{aligned} S_{XCI, X1_i}^x(f, N_s, L_s) &= \left(\frac{8}{9}\right)^2 \gamma^2 \Delta_f^3 \sum_{i=-\infty}^{\infty} \delta(f - i\Delta_f) \\ &\cdot \sum_{k,m,n \in X1_i} \sum_{k',m',n' \in X1_i} \mu(X1_i, N_s, L_s) \mu^*(X1_i, N_s, L_s) \\ &\cdot [4\mathbb{E}\{\nu_{x,k} \nu_{x,k'}^*\} \mathbb{E}\{\xi_{x,m}^* \xi_{x,n} \xi_{x,m'} \xi_{x,n'}^*\} + 2\mathbb{E}\{\nu_{x,k} \nu_{y,k'}^*\} \\ &\cdot \mathbb{E}\{\xi_{x,m}^* \xi_{x,n} \xi_{y,m'} \xi_{x,n'}^*\} + 2\mathbb{E}\{\nu_{x,k} \nu_{x,k'}^*\} \mathbb{E}\{\xi_{x,m}^* \xi_{x,n} \xi_{y,m'} \xi_{y,n'}^*\} \\ &+ 2\mathbb{E}\{\nu_{y,k} \nu_{x,k'}^*\} \mathbb{E}\{\xi_{y,m}^* \xi_{x,n} \xi_{x,m'} \xi_{x,n'}^*\} + \mathbb{E}\{\nu_{y,k} \nu_{y,k'}^*\} \\ &\cdot \mathbb{E}\{\xi_{y,m}^* \xi_{x,n} \xi_{y,m'} \xi_{x,n'}^*\} + \mathbb{E}\{\nu_{y,k} \nu_{x,k'}^*\} \mathbb{E}\{\xi_{y,m}^* \xi_{x,n} \xi_{y,m'} \xi_{y,n'}^*\} \\ &+ 2\mathbb{E}\{\nu_{x,k} \nu_{x,k'}^*\} \mathbb{E}\{\xi_{y,m}^* \xi_{y,n} \xi_{x,m'} \xi_{x,n'}^*\} + \mathbb{E}\{\nu_{x,k} \nu_{y,k'}^*\} \\ &\cdot \mathbb{E}\{\xi_{y,m}^* \xi_{y,n} \xi_{y,m'} \xi_{x,n'}^*\} + \mathbb{E}\{\nu_{x,k} \nu_{x,k'}^*\} \mathbb{E}\{\xi_{y,m}^* \xi_{y,n} \xi_{y,m'} \xi_{y,n'}^*\}]. \end{aligned} \quad (24)$$

This is now a six-dimensional sum and the complete auto-correlation function consist of nine terms. For ease of analysis, we simply rewrite (24) as

$$\begin{aligned} S_{XCI, X1_i}^x(f, N_s, L_s) &= \left(\frac{8}{9}\right)^2 \gamma^2 \Delta_f^3 \sum_{i=-\infty}^{\infty} \delta(f - i\Delta_f) \\ &\cdot \sum_{k,m,n \in X1_i} \sum_{k',m',n' \in X1_i} \{\mu(X1_i, N_s, L_s) \mu^*(X1_i, N_s, L_s)\} \\ &\cdot \sum_{i \in \{0,1,\dots,W-1\}^6} [A_{1,i}(k, m, n, k', m', n') \\ &+ A_{2,i}(k, m, n, k', m', n') + A_{3,i}(k, m, n, k', m', n') \\ &+ A_{4,i}(k, m, n, k', m', n') + A_{5,i}(k, m, n, k', m', n') \\ &+ A_{6,i}(k, m, n, k', m', n') + A_{7,i}(k, m, n, k', m', n') \\ &+ A_{8,i}(k, m, n, k', m', n') + A_{9,i}(k, m, n, k', m', n')], \end{aligned} \quad (25)$$

where $\mathbf{i} \triangleq (i_1, i_2, \dots, i_6)$ and

$$\begin{aligned} A_{1,i}(k, m, n, k', m', n') &\triangleq 4\Delta_f^3 \{\mathbb{E}\{a_{x,i_1} a_{x,i_4}^*\} \mathbb{E}\{b_{x,i_2}^* b_{x,i_3} b_{x,i_5} b_{x,i_6}^*\}\} \\ &\cdot e^{-j \frac{2\pi}{W} (ki_1 - mi_2 + ni_3 - k'i_4 + m'i_5 - n'i_6)}. \end{aligned} \quad (26)$$

The other coefficients $A_{j,i}(k, m, n, k', m', n')$ with $j = 1, 2, \dots, 9$ are similar to $A_{1,i}(k, m, n, k', m', n')$.

Note that under the assumption that the elements in the random vectors \mathbf{a}_n and \mathbf{b}_n are independent and identically distributed (i.i.d.) random variables, we have $\mathbb{E}\{\mathbf{a}_n\} = \mathbb{E}\{\mathbf{b}_n\} = 0$. Therefore, some combinations of $(i_1, i_2, i_3, i_4, i_5, i_6)$ result in zero contributions. For example, in the case of $i_1 = i_4 \neq i_2 = i_3 = i_5 \neq i_6$, we have

$$\begin{aligned} &\mathbb{E}\{a_{x,i_1} a_{x,i_4}^*\} \mathbb{E}\{b_{x,i_2}^* b_{x,i_3} b_{x,i_5} b_{x,i_6}^*\} \\ &= \mathbb{E}\{|a_{x,i_1}|^2\} \mathbb{E}\{|b_{x,i_2}|^2 b_{x,i_3}\} \cdot \mathbb{E}\{b_{x,i_6}^*\} \\ &= 0. \end{aligned}$$

From this follows that, any combinations of the first-order moment and other-order correlation are zero-contribution com-

binations. Therefore, we have four possible combinations

$$\begin{aligned}
\text{Case (1)} \quad & i_1 = i_4 \quad i_2 = i_3 = i_5 = i_6 \\
\text{Case (2)} \quad & i_1 = i_4 \quad i_2 = i_3 \quad i_5 = i_6, \\
\text{Case (3)} \quad & i_1 = i_4 \quad i_2 = i_5 \quad i_3 = i_6, \\
\text{Case (4)} \quad & i_1 = i_4 \quad i_2 = i_6 \quad i_3 = i_5.
\end{aligned} \tag{27}$$

Here we give a detailed derivation of the term $A_{1,i}(k, m, n, k', m', n')$ in (26). The others terms $A_{j,i}(k, m, n, k', m', n')$ with $j = 2, 3, \dots, 9$ can be derived following the same approach. As (27) shows, the second-order moment is the set of $i_1 = i_4$,

$$\begin{aligned}
\mathbb{E}\{\nu_{x,k}\nu_{x,k'}^*\} &= \Delta_f |P(k\Delta_f)|^2 \mathbb{E}\{|a_x|^2\} \sum_{i_1=i_4=0}^{W-1} e^{-j\frac{2\pi}{W}(k-k')i_1} \\
&= R_s |P(k\Delta_f)|^2 \mathbb{E}\{|a_x|^2\} (\delta_{k-k'-pW}),
\end{aligned} \tag{28}$$

where we have used $R_s = W\Delta_f$ and the $p \in \mathbb{Z}$.

Its 4th-order moment is given by

$$\begin{aligned}
\mathbb{E}\{\xi_{x,m}^* \xi_{x,n} \xi_{x,m'} \xi_{x,n'}^*\} &= \Delta_f^2 \mathcal{P}_{mnm'n'} \sum_{i_2, i_3, i_5, i_6=0}^{W-1} \mathbb{E}\{b_{i_2}^* b_{i_3} b_{i_5} b_{i_6}^*\} \\
&\quad \cdot e^{-j\frac{2\pi}{W}(-i_2m+i_3n+i_5m'-i_6n')},
\end{aligned} \tag{29}$$

where $\mathcal{P}_{mnm'n'} = P^*(m\Delta + f_c)P(n\Delta + f_c)P(m'\Delta + f_c)P^*(n'\Delta + f_c)$.

The calculation of the 4th-order moment can be split according to the classification in (27):

- **Case (1):**

$$\begin{aligned}
\mathbb{E}^{(1)}\{\xi_{x,m}^* \xi_{x,n} \xi_{x,m'} \xi_{x,n'}^*\} &= R_s \Delta_f \mathcal{P}_{mnm'n'} \mathbb{E}\{|b_x|^4\} \\
&\quad (\delta_{n-m+m'-n'-pW}).
\end{aligned} \tag{30}$$

- **Case (2):**

$$\begin{aligned}
\mathbb{E}^{(2)}\{\xi_{x,m}^* \xi_{x,n} \xi_{x,m'} \xi_{x,n'}^*\} &= \mathcal{P}_{mnm'n'} \mathbb{E}^2\{|b_x|^2\} \\
&\quad (R_s^2 \delta_{n-m-pW} \delta_{m'-n'-pW} - R_s \Delta_f \delta_{n-m+m'-n'-pW}).
\end{aligned} \tag{31}$$

- **Case (3):**

$$\begin{aligned}
\mathbb{E}^{(3)}\{\xi_{x,m}^* \xi_{x,n} \xi_{x,m'} \xi_{x,n'}^*\} &= \mathcal{P}_{mnm'n'} \mathbb{E}^2\{|b_x|^2\} \\
&\quad (R_s^2 \delta_{m'-m-pW} \delta_{n-n'-pW} - R_s \Delta_f \delta_{n-m+m'-n'-pW}).
\end{aligned} \tag{32}$$

- **Case (4):**

$$\begin{aligned}
\mathbb{E}^{(4)}\{\xi_{x,m}^* \xi_{x,n} \xi_{x,m'} \xi_{x,n'}^*\} &= \mathcal{P}_{mnm'n'} |\mathbb{E}\{b_x^2\}|^2 \\
&\quad (R_s^2 \delta_{-m-n'-pW} \delta_{m'+n-pW} - R_s \Delta_f \delta_{n-m+m'-n'-pW}).
\end{aligned} \tag{33}$$

Note that we removed the terms with $n = m$ or $n' = m'$ because they have been shown to contribute a frequency-flat and constant phase shift which could be compensated at the receiver. Adding up the contributions in (30)–(33), we obtain the solution of (26).

The $S_{\text{XCI},X1}^x(f, N_s, L_s)$ is induced by the integration regions X1. As for the other contributions, they can be calculated

through the same procedure, and related to different integration regions in Fig. 2. By combining all the XCI contributions, the XCI power coefficient can be obtained in x as

$$\begin{aligned}
\eta_{\text{ss},\text{XCI}}^x &\triangleq \frac{\sigma_{\text{XCI},x}^2}{P^3} = P^{-3} \int_{-\infty}^{\infty} S_{\text{XCI}}^x(f, N_s, L_s) |P(f)|^2 df \\
&= \left(\frac{8}{9}\right)^2 \frac{\gamma^2}{P^3} \left[\underbrace{R_s^3 [\Phi_4 \chi_{12}(f) + \Phi_5 \chi_{13}(f)] + R_s^2 \Phi_6 \chi_{14}(f)}_{\eta_{\text{ss},X1}^x} \right. \\
&\quad + \underbrace{R_s^3 [\Psi_5 \chi_{12}(f) + \Psi_6 \chi_{15}(f)] + R_s^2 \Psi_7 \chi_{14}(f)}_{\eta_{\text{ss},X2}^x} \\
&\quad \left. + \underbrace{R_s^3 [\Lambda_7 \chi_{11}(f) + \Lambda_8 \chi_{12}(f)] + R_s^2 \Lambda_9 \chi_{10}(f)}_{\eta_{\text{ss},X3}^x} \right] + \eta_{\text{ss},X4}^x,
\end{aligned} \tag{34}$$

the $\eta_{\text{ss},X4}^x$ is the NLI contribution of X4 region. The X4 region has a similar structure as the SCI region, and thus, we use $\bar{\eta}_{\text{ss},\text{SCI}}^x$ to denote $\eta_{\text{ss},X4}^x$ in (12). The proof of Theorem 1 is completed by combining the same kind of terms in (34).

APPENDIX B PROOF OF THEOREM 2

For the NLI contribution of MCI, we take the same approach as in [37]. The most important things is to determine the integration regions of the integrand χ_k , $k = 16, 17, \dots, 24$. In other words, the location of the two three triples (f_1, f_2, f_3) and (f'_1, f'_2, f'_3) need to be determined. Therefore, the MCI power coefficient can be obtained in x as

$$\begin{aligned}
\eta_{\text{ss},\text{MCI}}^x &= 2 \cdot \left(\frac{8}{9}\right)^2 \frac{\gamma^2}{P^3} \left[\underbrace{R_s^3 [\Phi_4 \chi_{16}(f) + \Phi_5 \chi_{17}(f)] + R_s^2 \Phi_6 \chi_{18}(f)}_{\eta_{\text{ss},M1}^x} \right. \\
&\quad + \underbrace{R_s^3 [\Phi_4 \chi_{19}(f) + \Phi_5 \chi_{20}(f)] + R_s^2 \Phi_6 \chi_{21}(f)}_{\eta_{\text{ss},M2}^x} \\
&\quad \left. + \underbrace{R_s^3 [\Lambda_7 \chi_{22}(f) + \Lambda_8 \chi_{23}(f)] + R_s^2 \Lambda_9 \chi_{24}(f)}_{\eta_{\text{ss},M3}^x} \right] + \bar{\eta}_{\text{M0}}^x,
\end{aligned} \tag{35}$$

where the main difference between MCI components and their similar XCI components is the integration limits. Under the assumption that the total number of channels is odd and all INT channels are sitting symmetrically about COI, the INT channels can be expressed as INT_i , $i = -(N_{ch} - 1)/2, \dots, -1, 1, \dots, (N_{ch} - 1)/2$. Due to the symmetry, we will derive a formula for one quadrant, and then multiply it by two. The M1, M2 and M3 are shown as follows:

- **M1: similar to X1**

We evaluate M1 in the domains located(?) in the second quadrant, parallel to f_2 . We obtain:

$$\begin{aligned}
f_1, f'_1 &\in \text{INT}_1, \quad f_2, f_3, f'_2, f'_3 \in \text{INT}_n, \\
n &= 1, 2, \dots, (N_{ch} - 1)/2
\end{aligned}$$

- **M2: similar to X1**

For the domains locating in the first quadrant, parallel to f_2 . We obtain:

$$f_1, f'_1 \in \text{INT}_1, \quad f_2, f_3, f'_2, f'_3 \in \text{INT}_n,$$

$$n = 2, 3, \dots, (N_{ch} - 1)/2$$

- M3: similar to X3

For the domains locating in the first quadrant, we obtain:

$$f_3, f'_3 \in \text{INT}_m, \quad f_1, f_2, f'_1, f'_2 \in \text{INT}_n,$$

$$m = 2, 3, \dots, (N_{ch} - 1)/2$$

$$n = \begin{cases} m/2, m \text{ is even} \\ (m \pm 1)/2, m \text{ is odd} \end{cases}$$

The proof of Theorem 2 is completed by combining (35) with Table. II and Table. III.

REFERENCES

- [1] Z. Liang, B. Chen, Y. Lei, G. Liga, and A. Alvarado, "Analytical prediction in long-haul optical transmission using general dual-polarization 4D formats," in *Eur. Conf. Opt. Commun.*, Sep. 2022, pp. 1–4.
- [2] F. Kschischang and S. Pasupathy, "Optimal nonuniform signaling for gaussian channels," *IEEE Trans. Inf. Theory*, vol. 39, no. 3, pp. 913–929, May. 1993.
- [3] G. Forney, R. Gallager, G. Lang, F. Longstaff, and S. Qureshi, "Efficient modulation for band-limited channels," *IEEE Journal on Selected Areas in Communications*, vol. 2, no. 5, pp. 632–647, Sep. 1984.
- [4] G. Welti and J. Lee, "Digital transmission with coherent four-dimensional modulation," *IEEE Trans. Inf. Theory*, vol. 20, no. 4, pp. 497–502, Jul. 1974.
- [5] G. Forney, "Multidimensional constellations. ii. voronoi constellations," *IEEE Journal on Selected Areas in Communications*, vol. 7, no. 6, pp. 941–958, 1989.
- [6] E. Agrell and M. Karlsson, "Power-efficient modulation formats in coherent transmission systems," *J. Lightw. Technol.*, vol. 27, no. 22, pp. 5115–5126, Nov. 2009.
- [7] E. Sillekens, G. Liga, D. Lavery, P. Bayvel, and R. I. Killey, "High-cardinality geometrical constellation shaping for the nonlinear fiber channel," *J. Lightw. Technol.*, vol. 40, no. 19, pp. 6374–6387, Oct. 2022.
- [8] K. Kojima, T. Yoshida, T. Koike-Akino, D. S. Millar, K. Parsons, M. Pajovic, and V. Arlunno, "Nonlinearity-tolerant four-dimensional 2A8PSK family for 5-7 bits/symbol spectral efficiency," *J. Lightw. Technol.*, vol. 35, no. 8, Apr. 2017.
- [9] A. I. A. El-Rahman and J. C. Cartledge, "Multidimensional geometric shaping for QAM constellations," in *Eur. Conf. Opt. Commun.*, Sep. 2017, pp. 1–3.
- [10] S. Goossens, Y. C. Gültekin, O. Vassilieva, I. Kim, P. Palacharla, C. Okonkwo, and A. Alvarado, "Introducing 4D geometric shell shaping for mitigating nonlinear interference noise," *J. Lightw. Technol.*, vol. 41, no. 2, pp. 599–609, Jan. 2023.
- [11] B. Chen, Y. Lei, G. Liga, Z. Liang, W. Ling, X. Xue, and A. Alvarado, "Geometrically-shaped multi-dimensional modulation formats in coherent optical transmission systems," *J. Lightw. Technol.*, vol. 41, no. 3, pp. 897–910, Feb. 2023.
- [12] T. Fehenberger, A. Alvarado, G. Böcherer, and N. Hanik, "On probabilistic shaping of quadrature amplitude modulation for the nonlinear fiber channel," *J. Lightw. Technol.*, vol. 34, no. 21, pp. 5063–5073, Nov. 2016.
- [13] J. Renner, T. Fehenberger, M. P. Yankov, F. Da Ros, S. Forchhammer, G. Böcherer, and N. Hanik, "Experimental comparison of probabilistic shaping methods for unrepeated fiber transmission," *J. Lightw. Technol.*, vol. 35, no. 22, pp. 4871–4879, Nov. 2017.
- [14] B. Chen, C. Okonkwo, H. Hafermann, and A. Alvarado, "Polarization-switching for nonlinearity-tolerant geometrically-shaped four-dimensional formats maximizing generalized mutual information," *J. Lightw. Technol.*, vol. 37, no. 14, pp. 3579–3591, Jul. 2019.
- [15] V. Oliari, B. Karanov, S. Goossens, G. Liga, O. Vassilieva, I. Kim, P. Palacharla, C. Okonkwo, and A. Alvarado, "High-cardinality hybrid shaping for 4D modulation formats in optical communications optimized via end-to-end learning," *arXiv preprint arXiv:2112.10471*, 2021. [Online]. Available: <https://arxiv.org/abs/2112.10471>
- [16] —, "Hybrid geometric and probabilistic shaping; is it really necessary?" in *Optica Advanced Photonics Congress 2022*, Jul. 2022, pp. 1–2.
- [17] A. Mecozzi, C. Clausen, and M. Shtaif, "Analysis of intrachannel nonlinear effects in highly dispersed optical pulse transmission," *IEEE Photon. Technol. Lett.*, vol. 12, no. 4, pp. 392–394, Apr. 2000.
- [18] H. Louchet, A. Hodzic, and K. Petermann, "Analytical model for the performance evaluation of dwdm transmission systems," *IEEE Photon. Technol. Lett.*, vol. 15, no. 9, pp. 1219–1221, Sep. 2003.
- [19] P. Poggiolini, A. Carena, V. Curri, G. Bosco, and F. Forghieri, "Analytical modeling of nonlinear propagation in uncompensated optical transmission links," *IEEE Photon. Technol. Lett.*, vol. 23, no. 11, pp. 742–744, Jun. 2011.
- [20] L. Beygi, E. Agrell, P. Johannisson, M. Karlsson, and H. Wymeersch, "A discrete-time model for uncompensated single-channel fiber-optical links," *IEEE Trans. on Commun.*, vol. 60, no. 11, pp. 3440–3450, Nov. 2012.
- [21] A. Carena, V. Curri, G. Bosco, P. Poggiolini, and F. Forghieri, "Modeling of the impact of nonlinear propagation effects in uncompensated optical coherent transmission links," *J. Lightw. Technol.*, vol. 30, no. 10, pp. 1524–1539, May 2012.
- [22] A. Mecozzi and R.-J. Essiambre, "Nonlinear shannon limit in pseudo-linear coherent systems," *J. Lightw. Technol.*, vol. 30, no. 12, pp. 2011–2024, Jun. 2012.
- [23] P. Johannisson and M. Karlsson, "Perturbation analysis of nonlinear propagation in a strongly dispersive optical communication system," *J. Lightw. Technol.*, vol. 31, no. 8, pp. 1273–1282, Apr. 2013.
- [24] R. Dar, M. Feder, A. Mecozzi, and M. Shtaif, "Properties of nonlinear noise in long, dispersion-uncompensated fiber links," *Optics Express*, vol. 21, no. 22, pp. 25685–25699, Nov. 2013.
- [25] A. Carena, G. Bosco, V. Curri, Y. Jiang, P. Poggiolini, and F. Forghieri, "EGN model of non-linear fiber propagation," *Optics Express*, vol. 22, no. 13, pp. 16335–16362, Jun. 2014.
- [26] R. Dar *et al.*, "Accumulation of nonlinear interference noise in fiber-optic systems," *Opt. Express*, vol. 22, no. 12, pp. 14199–14211, Jun. 2014.
- [27] G. Liga, A. Barreiro, H. Rabbani, and A. Alvarado, "Extending fibre nonlinear interference power modelling to account for general dual-polarisation 4D modulation formats," *Entropy*, vol. 22, no. 11, pp. 1–38, Nov. 2020.
- [28] H. Rabbani, M. Ayaz, L. Beygi, G. Liga, A. Alvarado, E. Agrell, and M. Karlsson, "Analytical modeling of nonlinear fiber propagation for four dimensional symmetric constellations," *J. Lightw. Technol.*, vol. 39, no. 9, pp. 2704–2713, May 2021.
- [29] H. Rabbani, H. Hosseinianfar, and M. Brandt-Pearce, "An enhanced analytical model of nonlinear fiber effects for four-dimensional symmetric modulation formats," *J. Lightw. Technol.*, vol. 40, no. 16, pp. 5567–5574, Aug. 2022.
- [30] H. Rabbani, H. Hosseinianfar, H. Rabbani, and M. Brandt-Pearce, "Analysis of nonlinear fiber kerr effects for arbitrary modulation formats," *J. Lightw. Technol.*, vol. 41, no. 1, pp. 96–104, Jan. 2023.
- [31] A. Alvarado and E. Agrell, "Four-dimensional coded modulation with bit-wise decoders for future optical communications," *J. Lightw. Technol.*, vol. 33, no. 10, pp. 1993–2003, May 2015.
- [32] A. Alvarado, T. Fehenberger, B. Chen, and F. M. J. Willems, "Achievable information rates for fiber optics: Applications and computations," *J. Lightw. Technol.*, vol. 36, no. 2, pp. 424–439, Jan. 2018.
- [33] D. Lavery, D. Ives, G. Liga, A. Alvarado, S. J. Savory, and P. Bayvel, "The benefit of split nonlinearity compensation for single-channel optical fiber communications," *IEEE Photon. Technol. Lett.*, vol. 28, no. 17, pp. 1803–1806, Sep. 2016.
- [34] P. Poggiolini, G. Bosco, A. Carena, V. Curri, Y. Jiang, and F. Forghieri, "The GN-model of fiber non-linear propagation and its applications," *J. Lightw. Technol.*, vol. 32, no. 4, pp. 694–721, Feb. 2014.
- [35] M. Secondini and E. Forestieri, "Scope and limitations of the nonlinear shannon limit," *J. Lightw. Technol.*, vol. 35, no. 4, pp. 893–902, Feb. 2017.
- [36] J. C. Cartledge *et al.*, "Digital signal processing for fiber nonlinearities," *Optics Express*, vol. 25, no. 3, pp. 1916–1936, Feb. 2017.
- [37] A. Carena, G. Bosco, V. Curri, Y. Jiang, and F. Forghieri, "On the accuracy of the GN-model and on analytical correction terms to improve it," *Annali Di Radiologia Diagnostica*, vol. 28, no. 6, p. 407, 2014.
- [38] G. Liga, B. Chen, A. Barreiro, and A. Alvarado, "Modeling of nonlinear interference power for dual-polarization 4D formats," in *Opt. Fiber Commun. Conf.*, Mar. 2021, pp. 1–3.

- [39] P. Poggiolini, "The GN model of non-linear propagation in uncompensated coherent optical systems," *J. Lightw. Technol.*, vol. 30, no. 24, pp. 3857–3879, Dec. 2012.
- [40] "Sphere packings of dimension 4," <https://codes.se/packings/4.htm>.
- [41] B. Chen, G. Liga, Y. Lei, W. Ling, Z. Huan, X. Xue, and A. Alvarado, "Shaped four-dimensional modulation formats for optical fiber communication systems," in *Opt. Fiber Commun. Conf.*, Mar. 2022, pp. 1–3.
- [42] M. Karlsson and E. Agrell, "Four-dimensional optimized constellations for coherent optical transmission systems," in *36th European Conference and Exhibition on Optical Communication*, sep. 2010, pp. 1–6.
- [43] P. Poggiolini, G. Bosco, A. Carena, V. Curri, Y. Jiang, and F. Forghieri, "A simple and effective closed-form GN model correction formula accounting for signal non-gaussian distribution," *J. Lightw. Technol.*, vol. 33, no. 2, pp. 459–473, Jan. 2015.
- [44] T. A. Eriksson, S. Alreesh, C. Schmidt-Langhorst, F. Frey, P. W. Berenguer, C. Schubert, J. K. Fischer, P. A. Andrekson, M. Karlsson, and E. Agrell, "Experimental investigation of a four-dimensional 256-ary lattice-based modulation format," in *Optical Fiber Communication Conference*. Optica Publishing Group, Mar. 2015, p. W4K.3.
- [45] D. Marcuse, C. Manyuk, and P. Wai, "Application of the Manakov-PMD equation to studies of signal propagation in optical fibers with randomly varying birefringence," *J. Lightw. Technol.*, vol. 15, no. 9, pp. 1735–1746, Sep. 1997.
- [46] A. Vannucci, P. Serena, and A. Bononi, "The RP method: a new tool for the iterative solution of the nonlinear schrodinger equation," *J. Lightw. Technol.*, vol. 20, no. 7, pp. 1102–1112, Jul. 2002.